JCB Journal of Cell Biology

ARTICLE

Nanoscopy reveals the layered organization of the sarcomeric H-zone and I-band complexes

Szilárd Szikora[1,2], Tamás Gajdos[2], Tibor Novák[2], Dávid Farkas[1,4], István Földi[1], Peter Lenart[3], Miklós Erdélyi[2], and József Mihály[1,2]

Sarcomeres are extremely highly ordered macromolecular assemblies where structural organization is intimately linked to their functionality as contractile units. Although the structural basis of actin and Myosin interaction is revealed at a quasiatomic resolution, much less is known about the molecular organization of the I-band and H-zone. We report the development of a powerful nanoscopic approach, combined with a structure-averaging algorithm, that allowed us to determine the position of 27 sarcomeric proteins in *Drosophila melanogaster* flight muscles with a quasimolecular, ∼5- to 10-nm localization precision. With this protein localization atlas and template-based protein structure modeling, we have assembled refined I-band and H-zone models with unparalleled scope and resolution. In addition, we found that actin regulatory proteins of the H-zone are organized into two distinct layers, suggesting that the major place of thin filament assembly is an M-line–centered narrow domain where short actin oligomers can form and subsequently anneal to the pointed end.

Introduction

Sarcomeres are the basic contractile units of muscles. Early polarized light microscopy studies defined the sarcomere as a repeating unit of the myofibril bordered by two Z-disks, with a regular defined banded structure of I-band, A-band, H-zone, and M-line (reviewed in Squire et al., 2005). EM has subsequently shown that these sarcomeric regions result from a precise ultrastructure composed of three major filament systems: F-actin, known as the thin-filament array; the thick filaments composed of Myosin; and an elastic filament system based on Titin (reviewed in Gautel and Djinović-Carugo, 2016). The Z-disks serve as anchoring sites for the oppositely oriented thin filaments of neighboring sarcomeric units, and the regions either side of the Z-disks, containing thin filaments but devoid of thick filaments, are known as the I-band. The central thin-filament-free area known as the H-zone contains the headless Myosin regions of the bipolar thick filaments. The M-line (midline) region, flanked by the H-zone, corresponds to cross-linking structures associated with keeping neighboring thick filaments of the A-band in register. Sarcomeres are arguably the largest, most complex, and highly ordered macromolecular assemblies known. Their ultrastructure has been well characterized by x-ray crystallography and various EM methods. Such studies have led to quasiatomic models of thin and thick filaments from a number of animal species (Hu et al., 2016; Sulbaran et al., 2015; von der Ecken et al., 2015; Wu et al., 2010). However, despite the wealth of information collected, the exact spatial arrangement of many of the major muscle proteins remained unknown. In addition, several key aspects of myofilament array formation and dynamics are not resolved. Acquiring a precise molecular architecture of these is indispensable in order to understand the details of sarcomere assembly and function in healthy and disease conditions.

Ultrastructural analyses of sarcomeres have so far relied primarily on EM, with the detection of specific proteins accomplished by immunogold labeling. However, achieving high-density immunogold labeling is challenging; sample preparation is time consuming and manual annotation of gold particle location is tedious. This makes it difficult to assess with precision the relative position of sarcomeric proteins. In contrast, fluorescent microscopy appears a much more versatile tool with which to study sarcomeric protein distribution. Although the diffraction limit prevents the precise localization of the sarcomeric substructures by confocal laser scanning microscopy, recent advances in fluorescence superresolution imaging provide spatial resolutions that are well below the diffraction limit (reviewed in Huang et al., 2009). Single-molecule localization microscopy (SMLM; reviewed in Klein et al., 2014), especially when combined with particle-averaging methods (reviewed in Sigal et al., 2018), can deliver localization maps of multiprotein

[1]Institute of Genetics, Biological Research Centre, Hungarian Academy of Sciences, Szeged, Hungary; [2]Department of Optics and Quantum Electronics, University of Szeged, Szeged, Hungary; [3]Max Planck Institute for Biophysical Chemistry, Göttingen, Germany; [4]Doctoral School in Biology, Faculty of Science and Informatics, University of Szeged, Szeged, Hungary.

Correspondence to József Mihály: mihaly.jozsef@brc.hu.

https://doi.org/10.1083/jcb.201907026

complexes with very high precision, attaining a virtual resolution equivalent to the scale of single proteins.

Genetic and biochemical studies of the asynchronous indirect flight muscles (IFMs) of *Drosophila melanogaster*, the overall structure of which is similar to that of vertebrate striated muscles, have already contributed much to our current understanding of muscle development and function (Schnorrer et al., 2010; Spletter et al., 2018). Because these muscles are not needed for viability, they have proved to be suitable for genetic studies and an array of functional assays. Importantly, the extremely regular, near-crystalline structure of IFM sarcomeres makes the flight muscles ideal candidates for structural studies. Such high structural order and the intrinsic mirror symmetry of the H-zone and Z-disk provide an opportunity for structural averaging of the sarcomeric components. Here, we report on a nanoscopic approach to visualize the protein distribution in subdiffraction-sized compartments of the IFM sarcomeres, i.e., the H-zone and I-band. We collected direct stochastic optical reconstruction microscopy (dSTORM; Heilemann et al., 2008) images of ∼9,000 sarcomeres and developed a new software tool to determine the precise location of 14 epitopes in the H-zone and 21 epitopes in the I-band. We have combined this comprehensive localization information with the results of former structural, biochemical, and genetic studies to compile a refined sarcomere model with previously unprecedented scope and resolution. In addition, we determined the position of the major sarcomeric landmarks and gained novel functional insights into Z-disk, I-band, M-line, and H-zone organization as well as the mechanisms of thin filament pointed-end elongation.

Results

Nanoscopic assessment of flight muscle sarcomeres

To determine the subsarcomeric localization of the major IFM proteins with high-resolution fluorescent microscopy techniques, we first compared three different types of nanoscopic approaches: structured illumination microscopy (SIM), stimulated emission and depletion (STED), and dSTORM (Fig. S1, A–E). These pilot experiments revealed that dSTORM, a SMLM-based approach (Betzig et al., 2006; Heilemann et al., 2008; Hess et al., 2006; Rust et al., 2006), delivers the highest resolution and reliability when applied to individual myofibrils (Fig. 1, A–F). To establish a reference model for the mature sarcomeres, myofibrils were isolated from the IFM of young adults (∼24 h after eclosion). Since highly specific antibodies (Table S1) are available against different components of the sarcomere and organic fluorophores exhibit certain advantageous characteristics (i.e., high brightness and photostability), we used conventional immunofluorescent labeling. As the focal plane is parallel to the myofibrils we acquired 2D projections of the sarcomeres. These reveal the lateral distribution of proteins at the H-zones and I-bands (Fig. 1, G and H; and supplemental figure PDF).

After establishing sample preparation and immunolabeling procedures optimal for the IFM myofibrils, we collected super-resolution images of thousands of sarcomeres and quantitatively analyzed the individual structures. Based on their distribution along the longitudinal axis of the myofibrils, we could classify the immunolabeling patterns obtained into three major categories: "double lines," "bands," or "gaps" (Fig. 2, A–E). After classification, filtering, and quality control, the localization information of the selected sarcomeric structures were exported into IFM Analyser, a newly developed software tool dedicated to retrieve epitope distribution information from raw localization data for quantitative measurements (for a description, see Materials and methods). While quantitative measurements were performed on individual structures, for visualization purposes, we used the IFM Analyser to align the localizations along the symmetry axes of the H-zone/I-band by rotation and translation before averaging them. The averaged images gave thorough representation of the longitudinal and transverse distribution of the individual protein targets (Fig. 1, F–H). Subsequently, the aligned and averaged images were used to generate pseudo-multicolor representations (Fig. 2, F and G).

To rule out the possibility of sample preparation artifacts, we compared the nanoscopic structures of isolated individual myofibrils to those of dissected intact flight muscles (Fig. S1, F–G′). This revealed nearly identical patterns, confirming that the individual myofibril preparations are perfectly suitable for our goal. Thus, we applied the myofibril staining procedure and the analysis pipeline outlined above to determine the position of 27 muscle protein epitopes (Fig. 1, G and H). Note that most proteins enrich either at the H-zone or the I-band, while a few are present at both places (and along the entire thin filament). We provide a visual summary of all protein structure, confocal and dSTORM image, epitope distribution, and molecular modeling data in the supplemental figure PDF. From this huge dataset, the following sections focus on the key findings regarding the sarcomeric landmarks; the molecular architecture of the Z-disk, I-band, M-line, and H-zone; and the mechanisms of actin filament elongation in the H-zone.

Defining sarcomeric reference points

The backbone of the thin filament is a helical F-actin polymer with an average axial repeat of 28 monomers in 13 turns, corresponding to a repeat size of 2 × 38.7 nm in the IFM (Fig. 3 K; Miller and Tregear, 1972; Reedy and Reedy, 1985; Schmitz et al., 1994). The actin filaments are polarized structures with their plus ends (also known as barbed ends) cross-linked in the Z-disk and capped by CapZ (a heterodimer of Cpa and Cpb), and with their minus ends (also known as pointed ends) facing toward the M-line, where they are capped by Tropomodulin (Tmod). The regular arrangement of IFM sarcomeres facilitates the direct visualization of Tmod and CapZ (marked by anti-Cpa; Amândio et al., 2014), as the thin filaments are aligned in parallel arrays that are in perfect register with each other.

To establish sarcomeric reference points, we determined the localization of both Tmod and Cpa and found that both display a double-line-type distribution of parallel lines along the Z-disks and M-lines, respectively (Figs. 3 A and 4 A). From the profile of the dSTORM images, we defined the epitope positions with respect to the center of the H-zone (Fig. 3 J) and I-band (Fig. 4 E). We also confirmed the position of the pointed ends by directly visualizing the F-actin filament array (Fig. 3, A and J). To complement these structural insights, we determined the width of

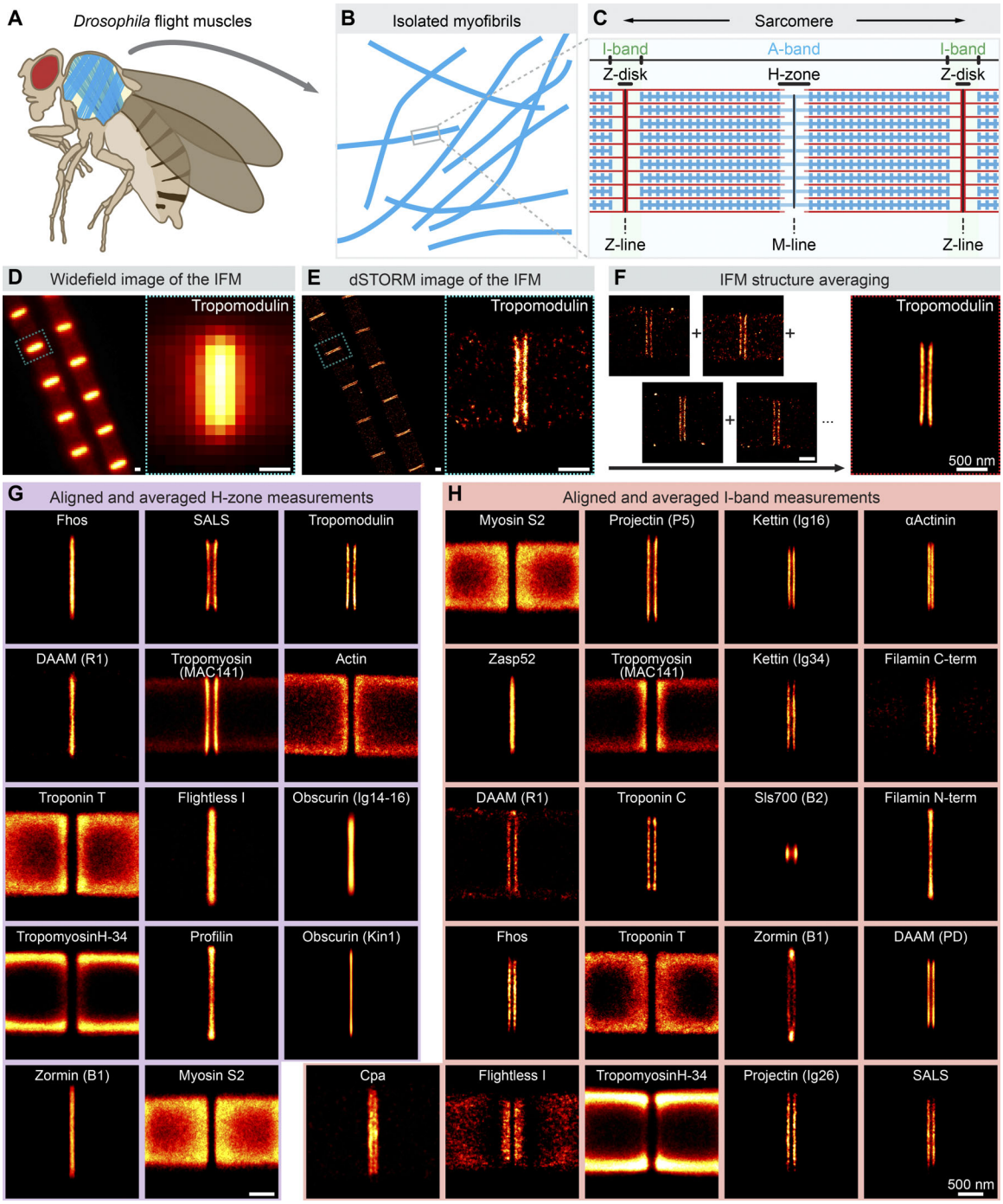

Figure 1. **dSTORM microscopy combined with structure averaging reveals the nanoscopic distribution of the sarcomeric proteins. (A–C)** The IFM, composed of dorsal longitudinal muscle fibers and dorsoventral muscle fibers (in blue; A), can be used to prepare individual myofibrils (B) exhibiting an extremely regular sarcomere organization (C) very similar to the one of vertebrate striated muscles. **(D and E)** Widefield (D) and dSTORM (E) images of flight muscle sarcomeres stained for Tmod. Insets, marked with cyan squares on the left, are shown in higher magnification on the right. **(F)** Tmod distribution after structure averaging of rotationally and translationally aligned dSTORM images. **(G and H)** Aligned and averaged images of sarcomeric proteins measured in the H-zone (G) and I-band (H; for a description, see text). Scale bars, 500 nm.

the I-band and the H-zone using a monoclonal antibody (Fyrberg et al., 1990) recognizing the S2 segment of the Myosin heavy chain (Mhc). This antibody labels the A-band almost uniformly and displays a gap-type distribution both in the I-band and H-zone with a half-gap width of 100.7 nm and 73.9 nm, respectively (Fig. 4, A and E; and see Fig. 7, A and E). Collectively, these results successfully established the positions of the key sarcomeric landmarks including the widths of the H-zone (133 nm), I-band (201.4 nm), and Z-disk (103 nm).

In addition, we aimed to determine the relative position and orientation of the Tropomyosin (Tm) and the regulatory Troponin (Tn) complex (composed of TnT, TnC, and TnI), attached

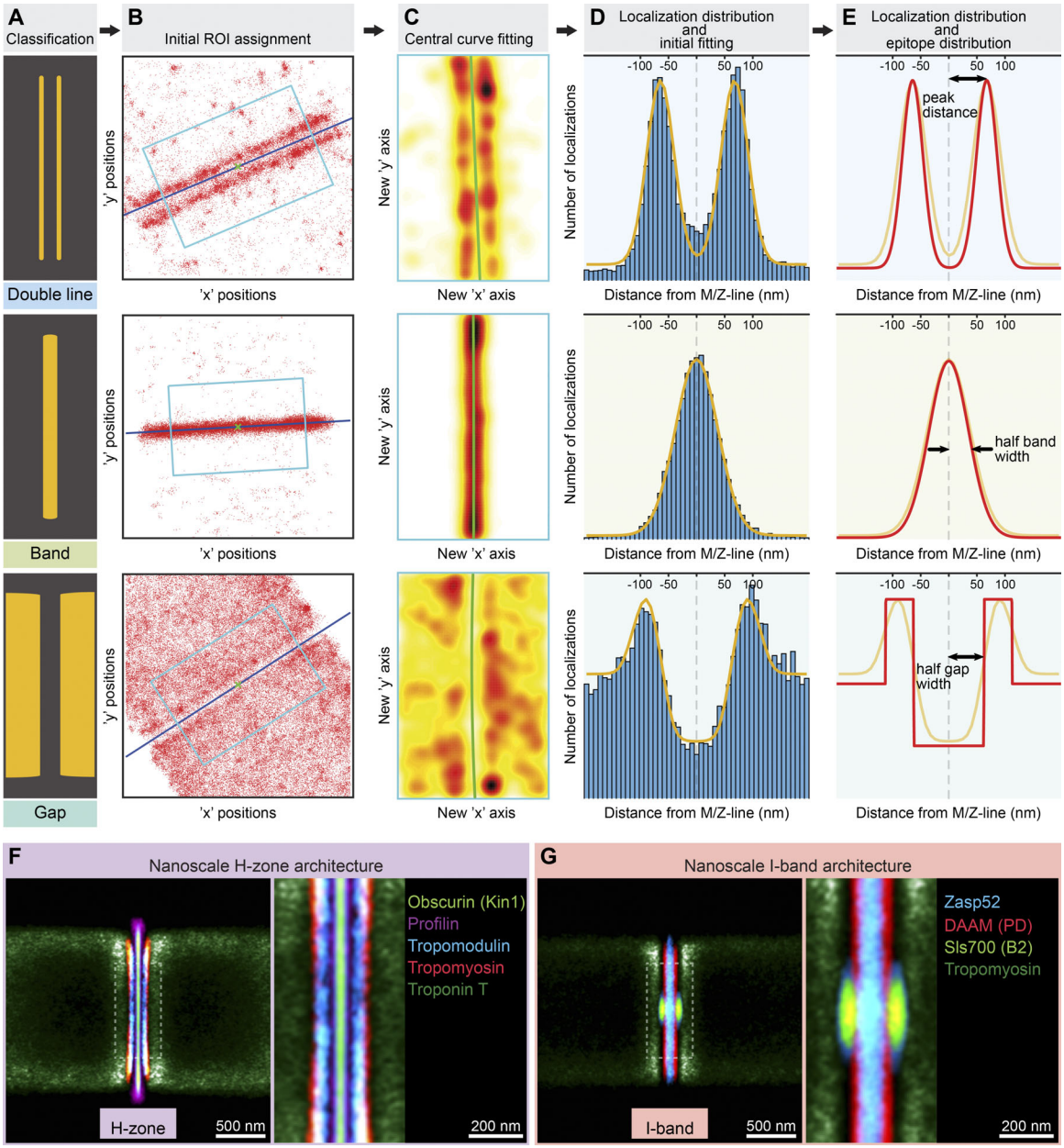

Figure 2. **Analysis pipeline of the raw localization data and aligned pseudo-multicolor representations of the H-zone/I-band structures.** Quantitative analysis is performed in multiple steps (for detailed description, see Materials and methods). **(A and B)** The analysis is performed according to the morphological classes (double lines, bands, or gaps; A) and starts with the region of interest (ROI) assignment (B). **(C)** Following that, the selected data (within the blue rectangle) is exported to the IFM Analyser toolset in which a central line (green line) corresponding to the symmetry axes of the H-zone/I-band is fitted on the localization densities. **(D)** Subsequently, a histogram is generated with a fitted curve (yellow line) equivalent to the localization distribution perpendicular to the central line (dashed line). **(E)** Finally, a theoretical curve (red line) is calculated, corresponding to an approximated epitope distribution and used for quantitative measurements. **(F and G)** Exploiting the mirror symmetry of the H-zone and the I-band, we merged the aligned and averaged images of independent proteins to generate examples of pseudo-multicolor representations of the H-zone (F) and I-band (G) structures. Scale bars, 500 nm. Insets are shown in higher magnification on the right. Scale bars, 200 nm.

to the Tm dimers. *Drosophila* IFM harbors three Tm isoforms: the standard striated muscle Tm127 isoform and two IFM-specific heavy Tms, TmH-33 and TmH-34. The heavy Tms contain Tm-homologous N-terminal domains and Pro-Ala-rich C-terminal domains of ~230 residues (Hanke and Storti, 1988; Karlik and Fyrberg, 1986). The TmHs are integrated into the thin filaments by their N-terminal parts, forming homo- and heterodimers between themselves and with Tm127 (Mateos et al., 2006). The N-termini of Tm are oriented toward the pointed end, where they interact with the C-terminus of the adjacent Tm dimer or the Tm-binding sites of Tmod (Greenfield et al., 2005). We examined the localization of Tm using the MAC141 antibody (Bullard et al., 1988), which is specific to a sequence close to the N-terminus, shared by all three Tm isoforms (Fig. S2 A; Cho et al., 2016; Clayton et al., 1998). The MAC141 staining is evident both in the I-band and H-zone. In the I-band, we found a

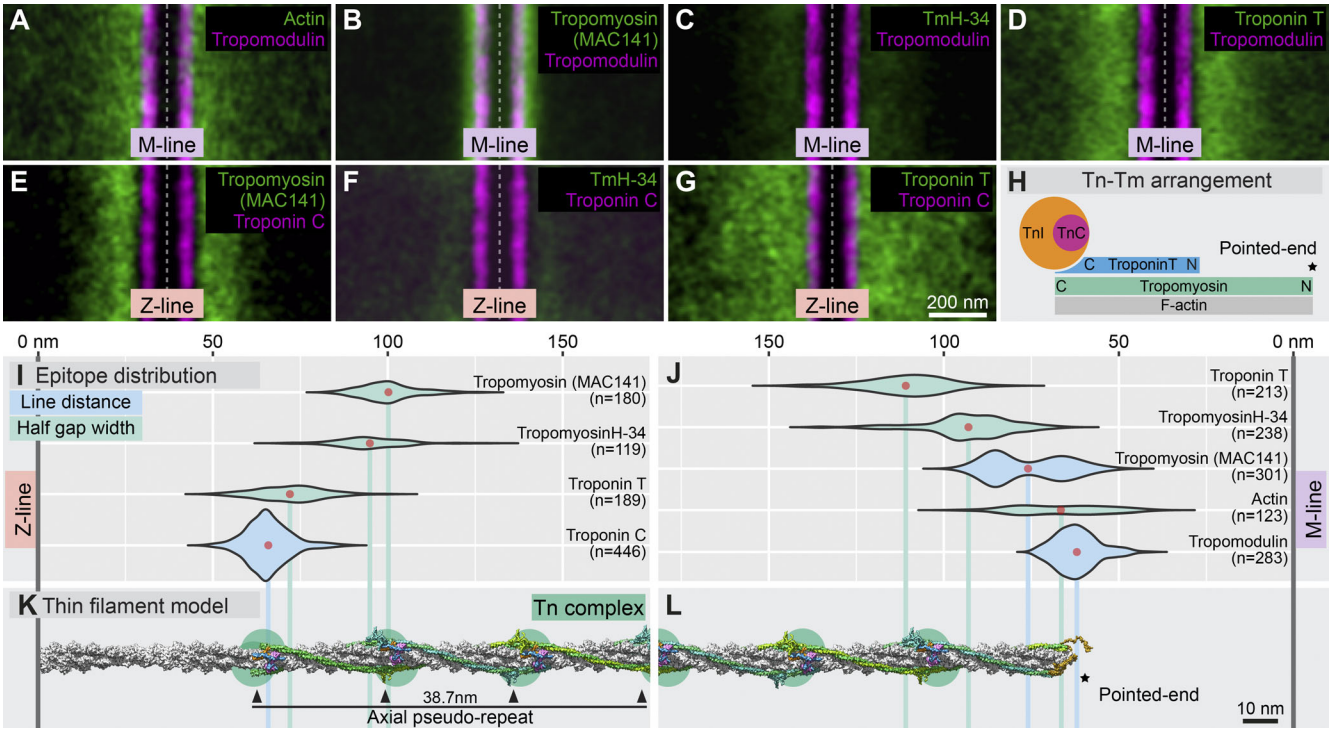

Figure 3. **Distribution of the major thin filament proteins at the nanoscopic scale. (A–G)** Pairwise alignment of thin filament components (including F-actin, Tmod, Tm, TmH-34, TnT, and TnC) in the H-zone (A–D) and I-band (E–G) regions. Scale bar, 200 nm. **(H)** Schematic of Tn complex–Tm arrangement along the thin filament. **(I and J)** Longitudinal epitope distributions relative to the Z- (I) and M-line (J), depicted as violin plots. Plot color indicates the corresponding protein density class and the applied measurements. Mean values are shown as red dots. **(K and L)** Molecular models of the thin filament from the I-band (K) and H-zone (L) regions. The models are scaled to the plots, with vertical lines marking the average epitope positions; F-actin is shown in gray, TnT in blue, TnC in magenta, TnI in orange, Tm in various shades of green, and Tmod in yellow. Scale bar, 10 nm.

gap-type distribution, whereas in the H-zone, the double lines appear to consist of two discrete peaks each, based on the line distance measurements (Fig. 3 J and Fig. S2, C and D). The monoclonal antibody against TnT displayed a gap-type distribution both in the I-band and in the H-zone (Fig. 3, D, G, I, and J), whereas the anti-TnC staining gave a double-line-type distribution in the I-band with a Z-line distance of 65 nm (Fig. 3, E, F, and I). These epitope positions in the I-band are entirely consistent with an N-terminal location of the Tm MAC141 epitope and indicate that the Tn complex binds the C-terminal part of Tm. Curiously, we noted that the MAC141 antibody does not label the thin filaments uniformly. Instead, it strongly labels the H-zone/A-band (Fig. 3 B) and I-band/A-band boundaries and weakly accumulates along the entire sarcomeres (Figs. 3 E and S2 B). A likely explanation is that the epitope is masked in the tightly packed A-band (Reedy and Bullard, 1996), and, accordingly, when C-terminus of the TmH molecules is removed by Igase digestion (Clayton et al., 1998), the Tm staining becomes nearly uniform along the sarcomeres (Fig. S2 B′). In the case of H-zone localization of Tm and TnT, we assume that the most M-ward Tn complex is missing from some of the thin filaments/myofibrils, which would explain the relatively large SD measured and would also be in line with the Igase treatment data.

Considering the position of the main reference points and localization of the Tm repeats, our results suggest that the Tn complex is positioned to the C-terminus of the Tm repeats (Fig. 3 H). Together, these results were integrated into the previously established IFM thin filament structure (Fig. 3, K and L; the molecular structure key is provided in Fig. 10; Wu et al., 2010) and served as a backbone for our subsequent structural modeling.

Z-disk organization and elastic filament localization in the I-band

The sarcomeres are flanked by Z-disks, cross-linking structures in which actin filaments of opposite polarity from neighboring sarcomeres interdigitate and are linked by connecting structures (Cheng and Deatherage, 1989; Deatherage et al., 1989). One of the main components of these Z-bridges are the α-Actinin homodimers that contain actin-binding domains at both ends of their central rod segment (reviewed in Luther, 2009). In vertebrate muscles, depending on fiber and muscle type, the Z-disks have a precise width determined by the number of α-Actinin layers, periodically positioned at every ∼19 nm (Luther et al., 2003). In the IFM, a single 104-kD muscle-specific α-Actinin isoform is expressed, and it displays a double-line-type distribution with an average Z-line distance of 39.3 nm (Fig. 4, B, D, and E). Hence, α-Actinin in the IFM forms only two layers separated by 78.6 nm. Besides α-Actinin, Zasp52 is another important Z-disk protein that is thought to interact with α-Actinin and cooperate in Z-disk formation (Katzemich et al., 2013; Liao et al., 2016). Using a monoclonal antibody (Table S1) against a muscle-specific

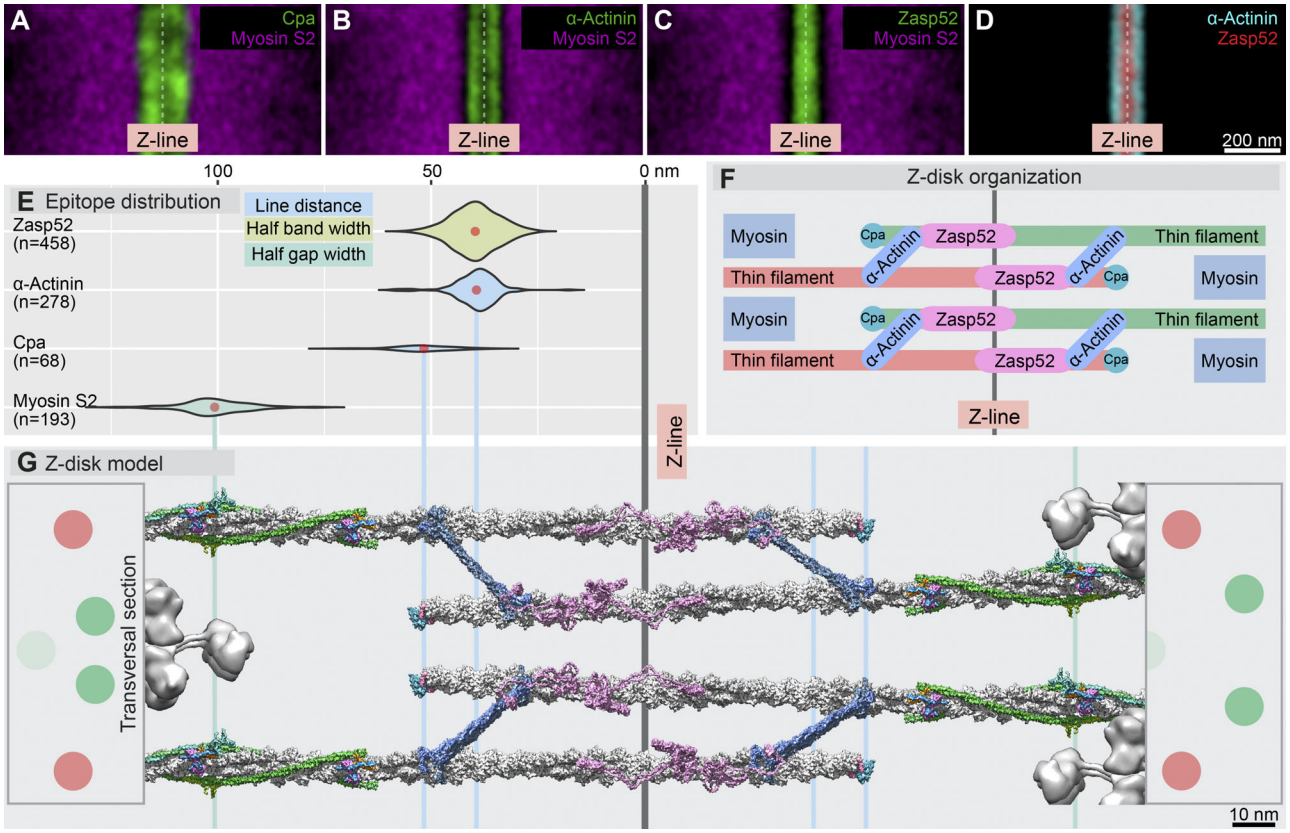

Figure 4. **Nanoscale arrangement of α-Actinin and Zasp52 at the Z-disk. (A–D)** Localization of the Z-disk proteins α-Actinin and Zasp52 as compared with the barbed end of the thin filaments marked by Cpa and to that of Myosin S2. Scale bar, 200 nm. **(E)** Longitudinal epitope distributions relative to the Z-line, depicted as violin plots. Plot color indicates the corresponding protein density class and the applied measurements. Mean values are shown as red dots. **(F)** Schematic Z-disk arrangement of α-Actinin and Zasp52. **(G)** Molecular model of the Z-disk, scaled to the plots on E, with vertical lines marking the average epitope positions. F-Actin is shown in gray, α-Actinin in blue, Zasp52 in magenta, Cpa in cyan, and Tm in green. Schematic transverse sections of the myofibril are shown on the left and right sides, representing the lattice structure of the thin filaments with red and green dots. Scale bar, 10 nm.

Zasp52 isoform (also known as Z(210); Chechenova et al., 2013) reveals a band-type distribution (Fig. 4, C–E) with a half bandwidth of 39.4 nm. However, a double-line-type distribution is evident in ∼20% of the individual images (supplemental figure PDF), and by assuming a hidden double line structure, we can determine the average epitope position more precisely (for description, see Materials and methods). This refines the approximate Z-line epitope distance to ∼24 nm, which positions it close to the Z-ward end of the α-Actinin dimer (Fig. 4, D–G), and provides further support for a Zasp52 role in regulating the Z-disk incorporation and positioning of α-Actinin.

In addition to the thin and thick filaments, striated muscles are equipped with an elastic system, made up of large modular proteins that link the thick filaments to the Z-disk. In vertebrate muscles, a single protein, Titin, extends from the Z-disk across the I-band and along half the length of the thick filament to the M-line. However, Titin is absent from the *Drosophila* genome. Instead, the *bent* (*bt*, also known as *projectin*) and *sallimus* (*sls*) genes express multiple isoforms of functionally similar proteins (Bullard et al., 2005). Kettin, the best-characterized Sls isoform, is composed of 35 Ig domains, separated by linker sequences, and is bound to the F-actin core of the thin filament. Its N-terminus is located in the middle of the Z-disk. This elongated molecule spans the I-band with its C-terminus facing the A-band, where it directly or indirectly attaches to the thick filaments (Bullard et al., 2006; van Straaten et al., 1999). To position this large, elongated protein in our model, two antibodies were used, one recognizing the Ig16 domain and the other one recognizing the Kettin C-terminal Ig34–Ig35 domains (Table S1; Kulke et al., 2001). As expected, both antibodies displayed a double-line-type distribution with an average Z-line distance of 49.2 nm and 66.8 nm, respectively (Fig. 5, A, B, and G–I). This arrangement is similar to the previously published immunoelectron micrographs (Burkart et al., 2007). However, our measurements clearly demonstrate that the C-terminus of Kettin is not close enough to be able to bind the A-band directly, which is consistent with the lack of a Myosin-binding domain (Machado and Andrew, 2000). While a direct interaction between Kettin and Myosin is highly unlikely, an indirect interaction is expected, as most of the high passive stiffness of the IFM is due to Kettin (Kulke et al., 2001). Projectin, mostly composed of repeated Ig and Fn motifs, is a prime candidate to mediate such an interaction (Bullard et al., 2006). Therefore, we next used two monoclonal antibodies (anti-Ig26 and P5; Lakey et al., 1990) to determine its subsarcomeric position. Both displayed a double-line-type distribution with an average Z-line

distance of 67.4 nm for anti-Ig26 and 79.4 nm for P5 (Fig. 5, E, F, and I). Because immunoelectron micrographs revealed that the N-terminal region of Projectin is located within the Z-disk (Ayme-Southgate et al., 2005), we predict that the epitope recognized by P5 is located further toward the C-terminus than Ig26, which is thought to be anchored to the thin filaments. The calculated contour length of Projectin is ∼320 nm, and when integrated into our molecular model, the C-terminus is located ∼130 nm from the Z-line, which overlaps with the edge of the A-band (i.e., end of the thick filaments; Fig. 5, J and K). Taken together, these data suggest that Kettin is restrained to an ∼132-nm-wide stripe within the ∼200-nm-wide I-band and therefore cannot make a direct contact with Myosin (Fig. 5 K). The observation that Tm is excluded from an ∼132-nm-wide stripe from the I-band is in line with the fact that Kettin and Tm bind F-actin in a mutually exclusive way (van Straaten et al., 1999).

We also determined the position of the two other Sls isoforms, Zormin and Sls(700), present in the IFM (Burkart et al., 2007). The B1 antibody, raised against the Ig4-Ig6 domains of Zormin (Table S1), displays a double-line-type distribution in the I-band, with an average Z-line distance of 57.8 nm (Fig. 5, D and I). Interestingly, these double lines converge into a spindle-like shape at the IFM periphery (Fig. 1 H). Anti-Sls(700) staining revealed a peculiar double-line-type distribution, with an average Z-line distance of 85 nm, which is, however, restricted to the myofibrillar core region (Fig. 5, C, H, and I). Whereas for Zormins, the lack of genetic and biochemical characterization hinders a precise placement of these molecules, the Sls(700) measurements suggest that its C-terminal domains overlap with the distal ends of the thick filaments and that they may attach to it (see Fig. 10 A). Importantly, as the diameter of IFM myofibrils grows by radial addition during pupal development (Mardahl-Dumesnil and Fowler, 2001; Orfanos and Sparrow, 2013), the localization of Sls(700) in the IFM core region indicates an early role during myofibrillogenesis.

Filamins (FLNs) cross-link the parallel thin filaments in the Z-disk

FLNs are large, actin filament cross-linking proteins that regulate Z-disk width in the IFM (Gonzalez-Morales et al., 2017). While vertebrates have three FLN isoforms (FLNa, FLNb, and FLNc), *Drosophila* produce at least 10 different isoforms, most of which are expressed in the IFM (Gonzalez-Morales et al., 2017). FLN-PM, a representative of one of the large isoforms, has a tandem Calponin homology domain containing an actin-binding region at its N-terminus, followed by 22 Ig repeats, among which the last one serves as a dimerization domain. To determine the sarcomeric localization of FLN, two different antibodies were used: C-terminus specific (Table S1; Li et al., 1999), which recognizes all isoforms, and N-terminus specific, raised against residues 132–482 (Table S1; Külshammer and Uhlirova, 2013). In addition to a largely uniform pattern spanning the entire myofibril (supplemental figure PDF), the C-terminal antibody revealed a double-line-type distribution at the Z-disk with an average Z-line distance of 54.3 nm (Fig. 6, A, C, and D). In contrast to this, the N-terminus–specific antibody displayed a "band"-type distribution with an average half bandwidth of 39.4 nm (Fig. 6, B–D). Presuming that this band is formed by the N-termini of FLN from adjoining sarcomeres, we can estimate the average epitope positions with higher precision (for description, see Materials and methods). This gives an approximate Z-line epitope distance of ∼23 nm.

These data clearly place the N-termini of FLN dimers to a more central Z-line location compared with the C-termini (Fig. 6 E), which is positioned remarkably close (4.2 nm M-ward) to the end of the thin filaments. The orientation of FLN dimers, combined with molecule structure predictions, protein interaction data (Gonzalez-Morales et al., 2017), and Z-disk lattice structure (Vigoreaux, 2007), not only allows the precise placement of FLN into our sarcomere model but also suggests a role in cross-linking of the parallel running thin filaments of the Z-disk (Fig. 6 F). Moreover, this position is relevant with regard to earlier studies of Z-disk organization in honeybee IFMs (Cheng and Deatherage, 1989; Deatherage et al., 1989; Rusu et al., 2017). These authors found various connecting EM densities between actin filaments that can be described as five compact domains (C1–C5). Whereas its molecular nature remains obscure, the C4 density is known to cross-link actin filaments of the same polarity and to have a threefold symmetry. Domain C4 consists of a central hub from which three arms radiate out to three actin filaments of the same polarity. Based on our measurements, FLN is likely to correspond to the C4 density, or be at least one component of it. Provided that the *Drosophila* and honeybee Z-disks exhibit very similar structural organization at the EM level (Koana and Hotta, 1978; Reedy and Beall, 1993), our model suggests that the "hub" close to the filament termini corresponds to the globular C-terminal part of FLM, while the "arms" are the actin-binding rod domains facing toward the Z-disk core region (Fig. 6 F). The number of arms radiating from the C4 density indicates that the hub contains more than one FLM dimer. Finally, we note that recent work revealed an interaction between Sls and the Ig 19–22 region of FLN (Gonzalez-Morales et al., 2017), and this finding is entirely compatible with our model. Thus, high-resolution analysis of this major Z-disk component provided an example for the power of our nanoscopic approach, where collection of precise localization data was instrumental in our reconstruction of a key sarcomeric structure.

The major M-line protein Obscurin displays an overlapping antiparallel arrangement in the H-zone

In *Drosophila* IFMs, Obscurin, a large Titin-like protein (Young et al., 2001), is specifically enriched in the M-line. Here, it plays a key role in sarcomere organization by controlling the incorporation and symmetry of the Myosin filaments (Katzemich et al., 2012). Of the five *Drosophila* Obscurin isoforms, two (A and C) are present in the IFM (Katzemich et al., 2012). The ∼475-kD Obscurin A is composed of an N-terminal SH3 domain, followed by Rho-GEF signaling domains (DH-PH domains), 21 Ig-like domains, two fibronectin-like (Fn3) domains, and two kinase domains close to the C-terminus. The smaller ∼370-kD Obscurin C, primarily present in mature flies, lacks the SH3 and DP-PH domains.

Two antibodies were used to determine the position and orientation of Obscurin within the H-zone. The first was raised against the Ig14–16 region (Burkart et al., 2007), and the second

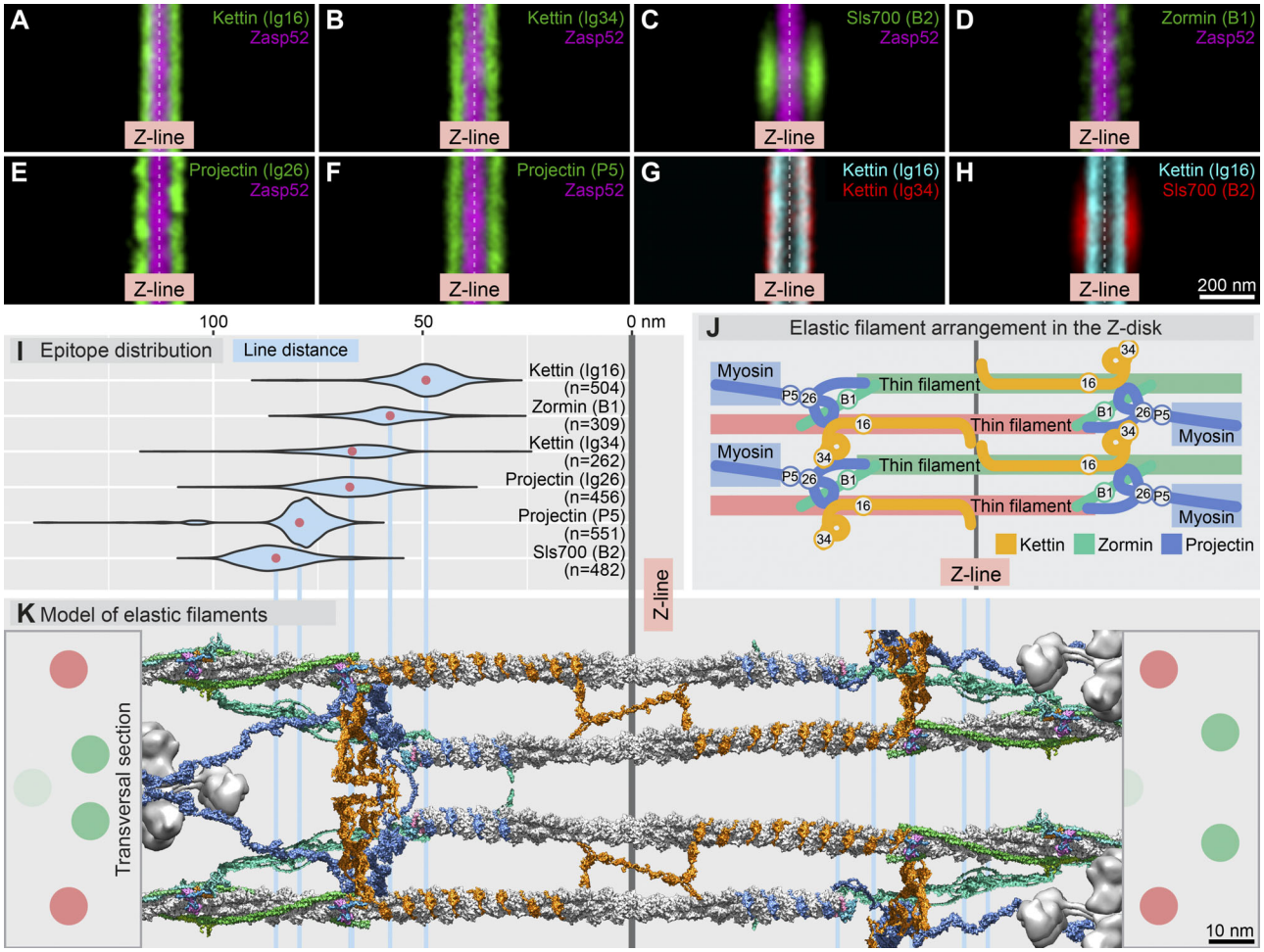

Figure 5. **Nanoscale arrangement of the elastic protein components of the I-band. (A–F)** Distribution of the elastic protein epitopes Kettin (Ig16 and Ig34), Sls700 (B2), Zormin (B1), and Projectin (Ig26 and P5) as compared with Zasp52. **(G and H)** Pairwise alignment of Kettin (Ig16) to that of (**G**) Kettin (Ig34) and (**H**) Sls700 (B2). Scale bar, 200 nm. **(I)** Longitudinal epitope distributions (i.e., line distances of the elastic proteins relative to the Z-line), depicted as violin plots. Mean values are shown as red dots. **(J)** Schematic arrangement of the measured elastic filaments and their distinguished epitopes in the I-band. **(K)** Molecular model of elastic protein organization in the I-band/Z-disk region, scaled to the plots on I, with vertical lines marking the average epitope positions. F-Actin is shown in gray, Projectin in blue, Kettin in orange, Zormin in teal, and Tm in green. Schematic transversal sections of the myofibril are shown on the left and right sides, representing the lattice structure of the thin filaments with red and green dots. Scale bar, 10 nm.

recognizes the kinase 1 domain (hereafter referred to as Kin1; Katzemich et al., 2012). Both antibodies display a band-type distribution in the middle of the H-zone with half bandwidths of 32.7 nm for the Ig14–16 antibody and 24.7 nm for the Kin1 antibody (Fig. 7, A–C and E). These epitope distributions suggest that Obscurin has a mirror symmetric pattern and that the C-termini are closer to the H-zone center, while the N-termini face toward the thin filaments (Fig. 7 F). Presuming a symmetric distribution, we can estimate the average epitope positions more precisely (for a description, see Materials and methods). This refines the approximate M-line epitope distance as ∼19 nm and ∼9 nm, respectively. An overlapping, antiparallel Obscurin arrangement would perfectly account for these values. As our template-based structure prediction suggests that the contour length is close to ∼130 nm for Obscurin A and ∼110 nm for Obscurin C, the predicted size and orientation places the N-terminus of Obscurin near the thin filament pointed ends (Fig. 7 G). From this we propose that Obscurin may interact directly with the thin filaments and/or indirectly through pointed end regulator proteins.

Obscurin is required for the M-line accumulation of the Sls isoform, Zormin (Burkart et al., 2007; Katzemich et al., 2012). Using the B1 (anti-Zormin) antibody, we obtained a double-line-type distribution, with an M-line distance of 30 nm, indicating a symmetrical protein arrangement (Fig. 7, D and E). Based on our structure prediction, the contour length of Zormin is ∼85 nm and, therefore, it can easily overlap with the proximal ends of the thin filaments. Together, by adding novel geometric constrains, these measurements provide a refined H-zone backbone structure.

Actin regulatory proteins of the H-zone are organized into two distinct layers

Labeled monomer incorporation studies in muscle cells suggested that the sarcomeric actin filaments are dynamic at both ends (Littlefield et al., 2001). Unexpectedly, blocking of barbed

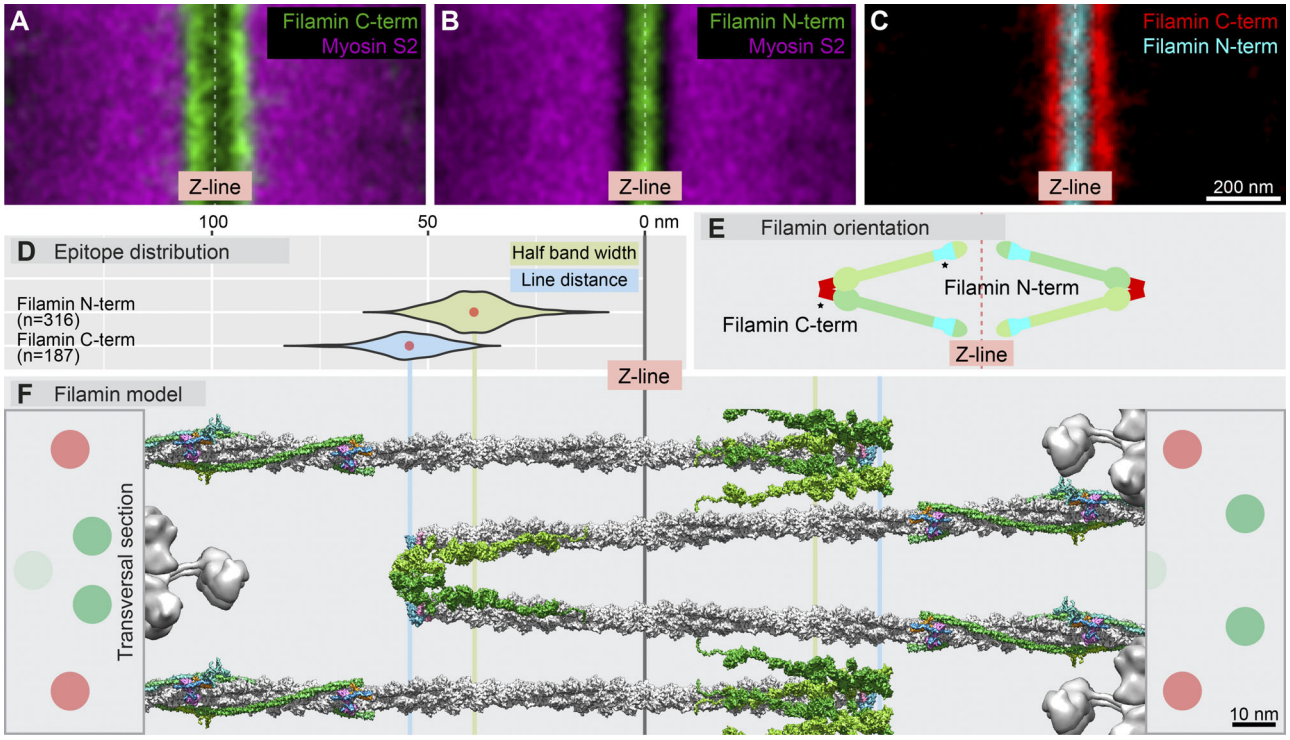

Figure 6. **FLN cross-links the parallel actin filaments at the Z-disk. (A–C)** Localization of FLN C-terminus and N-terminus compared with Myosin S2 and with each other. Scale bar, 200 nm. **(D)** Longitudinal epitope distributions relative to the Z-line, depicted as violin plots. Plot color indicates the corresponding protein density class and the applied measurements. Mean values are shown as red dots. **(E)** Schematic of FLN orientation at the Z-disk. **(F)** Molecular model of the Z-disk scaled to the plots on E, with vertical lines marking the average epitope positions. On the left side, there are two parallel actin filaments (in gray) cross-linked by a FLN dimer (in green); Cpa (in cyan) indicates the barbed end of the actin filaments. Schematic transversal sections of the myofibril are shown on the left and right sides, representing the lattice structure of the thin filaments (red and green dots). Scale bar, 10 nm.

end dynamics does not arrest actin filament elongation, while blocking of pointed end dynamics prevents filament growth. Therefore, in contrast to nonmuscle cells, actin filaments elongate from their pointed end during myofibrillogenesis (Littlefield et al., 2001; Mardahl-Dumesnil and Fowler, 2001) with an apparently unknown mechanism. Nevertheless, a number of proteins have already been linked to the regulation of sarcomeric actin dynamics and thin-filament elongation. We determined the distribution of this set of actin regulators, including the pointed end capping protein Tmod (Mardahl-Dumesnil and Fowler, 2001), the tandem WH2 domain containing SALS protein (Bai et al., 2007), the two formins (DAAM and Fhos; Molnár et al., 2014; Shwartz et al., 2016), the G-actin–binding Profilin protein (Kooij et al., 2016), and the Gelsolin family member Flightless-I (FliI; Miklos and De Couet, 1990).

As expected, the pointed-end–binding Tmod protein is excluded from the I-band, whereas the barbed-end–binding formin proteins DAAM and Fhos are clearly present there. The antibody specific to the N-terminus of the large DAAM isoform (PD; Table S1) and the R1 antibody raised against its C-terminus (Table S1 and Fig. S3, A–F) both displayed a double-line-type distribution with an average Z-line distance of 50.6 nm and 60.5 nm, respectively (Fig. 8, A–C, F, and I). Similarly, Fhos, the single *Drosophila* FHOD (formin homology domain-containing protein) subfamily orthologue, also displayed a double-line-type distribution in the I-band, with an average Z-line distance of 52.9 nm (Fig. 8, D, F, and I). The potential formin binding partner FliI (Higashi et al., 2010) is present near the Z-disk as well. It is found in two pairs of bands, representing a unique and peculiar pattern. The average Z-line distance of the Z-ward set of bands is 69.7 nm, whereas the other set of lines (only noticeable on the averaged representations) is located ∼60 nm M-ward (Fig. 8, G–I). As to SALS, initially characterized as a thin filament elongation factor, our nanoscopic assessment revealed a double-line-type distribution in the I-band, with an average Z-line distance of 46.7 nm (Fig. 8, E, F, and I). Collectively, these measurements support the barbed end association of these actin regulators (Fig. 8, J and K).

In addition to their I-band localization, but still consistent with phenotypic data (Bai et al., 2007; Miklos and De Couet, 1990; Molnár et al., 2014; Shwartz et al., 2016), DAAM, Fhos, SALS, FliI and Profilin were all found to be enriched in the H-zone as well. Of these, SALS displays a nearly perfect colocalization with that of Tmod with an average M-line distance of 64.2 nm (Fig. 9, A and I), a location only 2.2 nm Z-ward from Tmod. As to formins, when analyzed at the nanoscopic level, Fhos and DAAM both displays a band-type distribution in the H-zone with an average half bandwidth of 22.1 nm for Fhos and 29.9 nm for DAAM (Fig. 9, C, D, F, and I). Localization of these formins in a narrow stripe in the middle of the H-zone, in a seemingly F-actin-free area (Fig. 9, J and K), is intriguing. Since they cannot be connected to the actin filaments, we tested

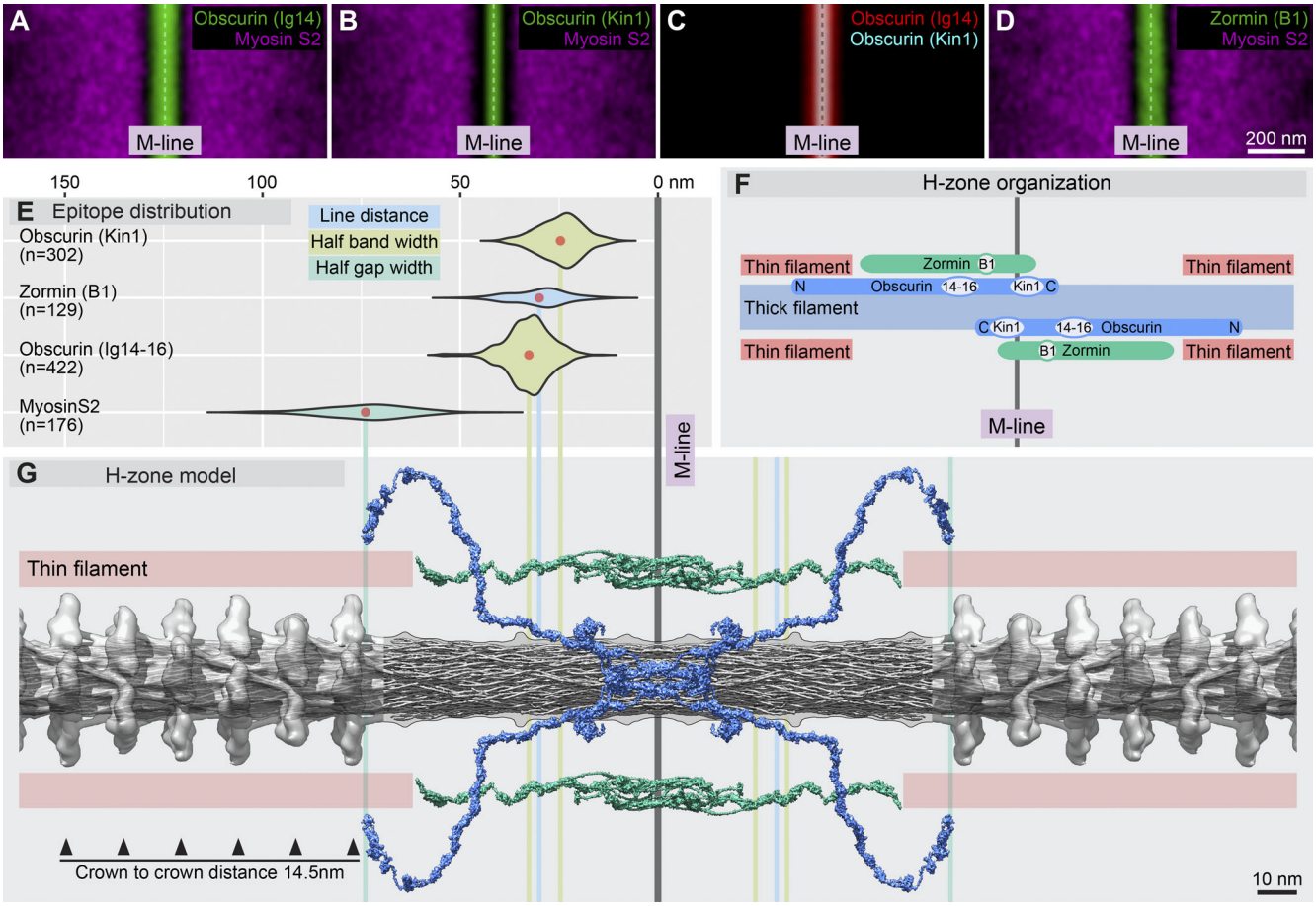

Figure 7. **Obscurin displays an overlapping antiparallel arrangement in the H-zone. (A–D)** Localization of two Obscurin epitopes (Ig14 and Kin1), as compared with Myosin S2 and each other, as well as that of Zormin (B1) compared with Myosin S2. Scale bar, 200 nm. **(E)** Longitudinal epitope distributions relative to the M-line, depicted as violin plots. Plot color indicates the corresponding protein density class and the applied measurements. Mean values are shown as red dots. **(F)** Schematic organization of Obscurin and Zormin in the H-zone. **(G)** Molecular model of the central region of sarcomere, scaled to the plots on E, with vertical lines marking the average epitope positions. Myosin is shown in gray, Obscurin in blue, and Zormin in teal. Note that Obscurin and Zormin are both in a position to contact the pointed end of the thin filaments (pink rectangles). Scale bar, 10 nm.

whether removal of myofibrillar Myosin influences their localization. We found that in IFM of *Mhc*^{10} homozygous mutant flies, the DAAM signal became completely diffuse (Fig. S3, H and I), suggesting that at least DAAM localization depends on Myosin.

Profilin-actin is the major G-actin source for formin-mediated actin assembly, and accordingly, overexpression of human Profilin in the IFM induces thin filament overgrowth (Kooij et al., 2016). While the latter study suggested that endogenous Profilin accumulates at the Z-disk, our comprehensive developmental profiling (based on confocal analysis) revealed an enrichment that appears stronger in the H-zone from the pupal till the adult stages (Fig. S3, G and G′). Consistently, visualization of the nanoscopic distribution of Profilin revealed a band-type pattern centered on the M-line with an average half bandwidth of 45.6 nm (Fig. 9, B, F, and I). This arrangement, combined with the observation that monomeric actin is present in the H-zone (as judged by fluorescent DNaseI and actin C4 staining; Mannherz et al., 1980; Fig. S3 and supplemental figure PDF), supports a Profilin-actin–facilitated pointed-end elongation hypothesis. Based on its myofibril phenotype (Miklos and De Couet, 1990), FliI is also involved in thin filament elongation, and remarkably, it was shown to associate with formins in various cell types and contribute to their activation (Higashi et al., 2010). We detected a pronounced band-type FliI accumulation in the H-zone, with an average half bandwidth of 38.9 nm (Fig. 9, E–I). This location is undoubtedly M-wards from SALS (the calculated distance is 22.1 nm), while it almost completely overlaps with that of Profilin and partly overlaps with the formins Fhos and DAAM.

These findings revealed that the proteins linked to pointed-end elongation accumulate into two clearly distinct spatially confined domains within the H-zone, separated by at least 15–20 nm (Fig. 9, J and K). In particular, Tmod and SALS are localized directly at the pointed end, whereas the two formins and two associated factors are highly enriched in a more central/M-ward location.

Discussion

The extremely regular sarcomeric structure of the *Drosophila* IFM allowed us to develop a powerful single-molecule localization system combined with structure averaging to determine the position of a large number of muscle proteins with a previously unprecedented localization precision of ∼5–10 nm. Whereas the

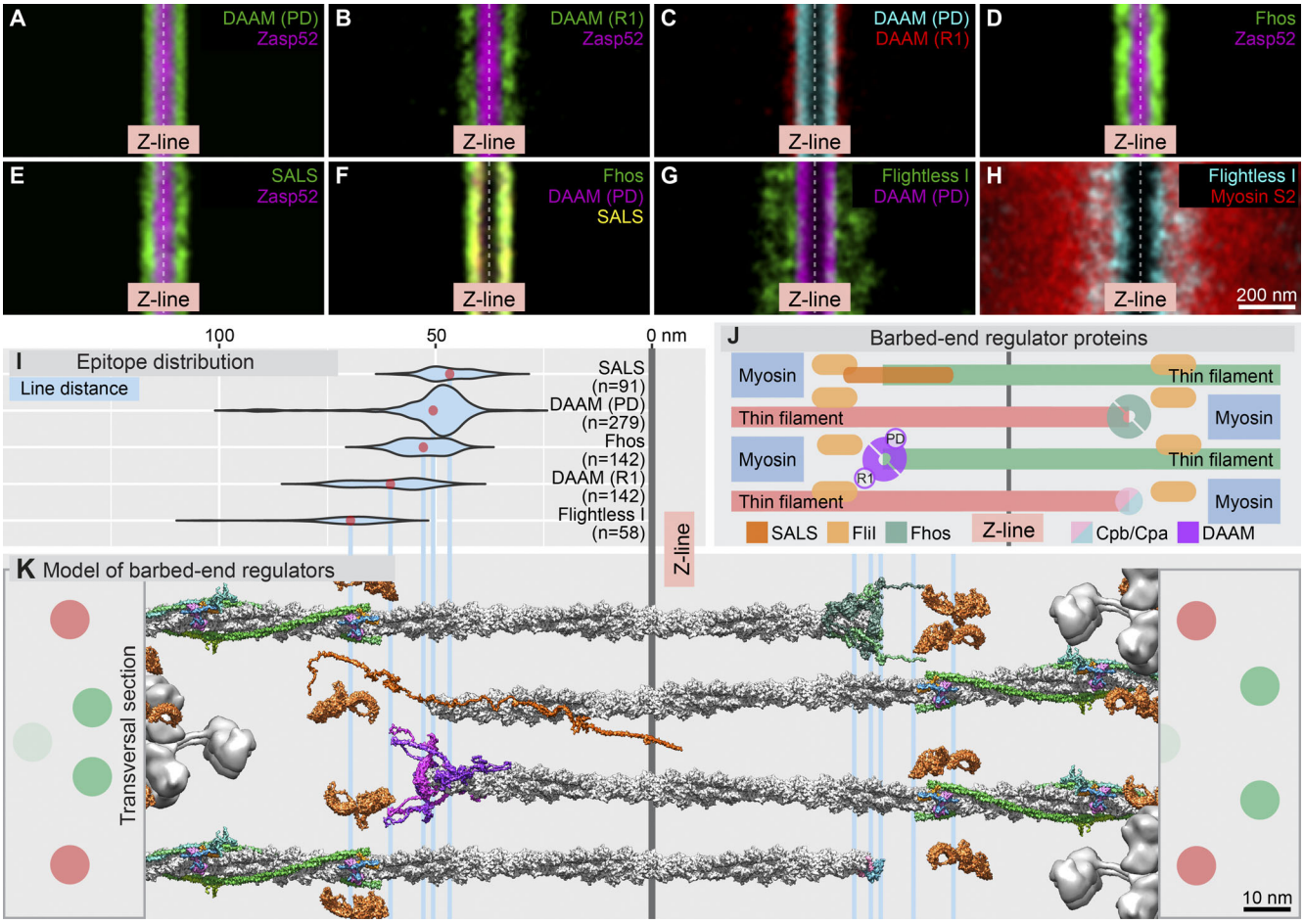

Figure 8. **Nanoscale arrangement of the actin regulatory proteins at the Z-disk. (A–H)** Distribution of the actin-binding protein DAAM (PD and R1), Fhos, SALS, and FliI as compared with Zasp52 (A, B, D, and E), each other (C, F, and G), or Myosin S2 (H) at the Z-disk. Scale bar, 200 nm. **(I)** Longitudinal epitope distributions (i.e., line distances of the actin regulatory proteins relative to the Z-line), depicted as violin plots. Mean values are shown as red dots. **(J)** Schematic arrangement of the potential barbed-end regulatory proteins at the Z-disk. **(K)** Molecular model of actin regulatory protein distribution in the I-band/Z-disk region, scaled to the plots on I, with vertical lines marking the average epitope positions. F-Actin is shown in gray, DAAM in magenta, Fhos in light green, FliI in orange, SALS in red orange, Tm in green, and Cpa in cyan. Schematic transversal sections of the myofibril are shown on the left and right sides, representing the lattice structure of the thin filaments (red and green dots). Scale bar, 10 nm.

actin-myosin overlap in the A-band of the sarcomeres is well understood, molecular organization of the I-band and the H-zone is much less well characterized, and thus, we focused our studies on these regions. From our analysis of >9,000 sarcomeres, we localized several Z-disk–, M-line–, thin filament–associated and elastic proteins. From these data, we have assembled comprehensive models of the H-zone and I-band complexes (Fig. 10) using the known PDB-deposited structures as well as template-based protein structure modeling and the IFM lattice structure (Vigoreaux, 2007) as a framework.

The first important benefit was that we could determine precise positions of all key sarcomeric reference points. These include the plus and minus ends of the thin filaments, the thick filament ends, and the positions of the M- and Z-lines. Implicitly, these provide the widths of the I-band and H-zone. These landmarks were instrumental in revealing the molecular organization of the thin filaments by unambiguously determining the orientation of the Tm–Tn complex. Furthermore, in agreement with former *Lethocerus indicus* work (Wendt et al., 1997), our results confirm that the Tn complex is located at the end of the Tm dimers. We also determined the precise locations of numerous Z-disk proteins, including α-Actinin, ZASP52, FLN, Projectin, and Sls isoforms. The localization atlas produced was used to support our molecular reconstruction of the Z-disk and facilitate the identification of the previously observed connecting EM densities (Cheng and Deatherage, 1989; Deatherage et al., 1989), such as in the case of FLN that we propose to be part of/form the C4 density. Moreover, the high-resolution analysis of FLN illustrates that the collection of nanoscopic localization data can be a remarkably powerful tool in molecular reconstruction that could help us to better understand the function of an important muscle protein.

In building a detailed model of the H-zone complex, we identified novel architectural features of the two major structural components of the H-zone, Obscurin and Zormin. Our data argue that the N-terminus of the Titin-like protein Obscurin faces the A-band. Therefore, it is in a position to interact with thin filament pointed-end regulatory proteins. Replacement of

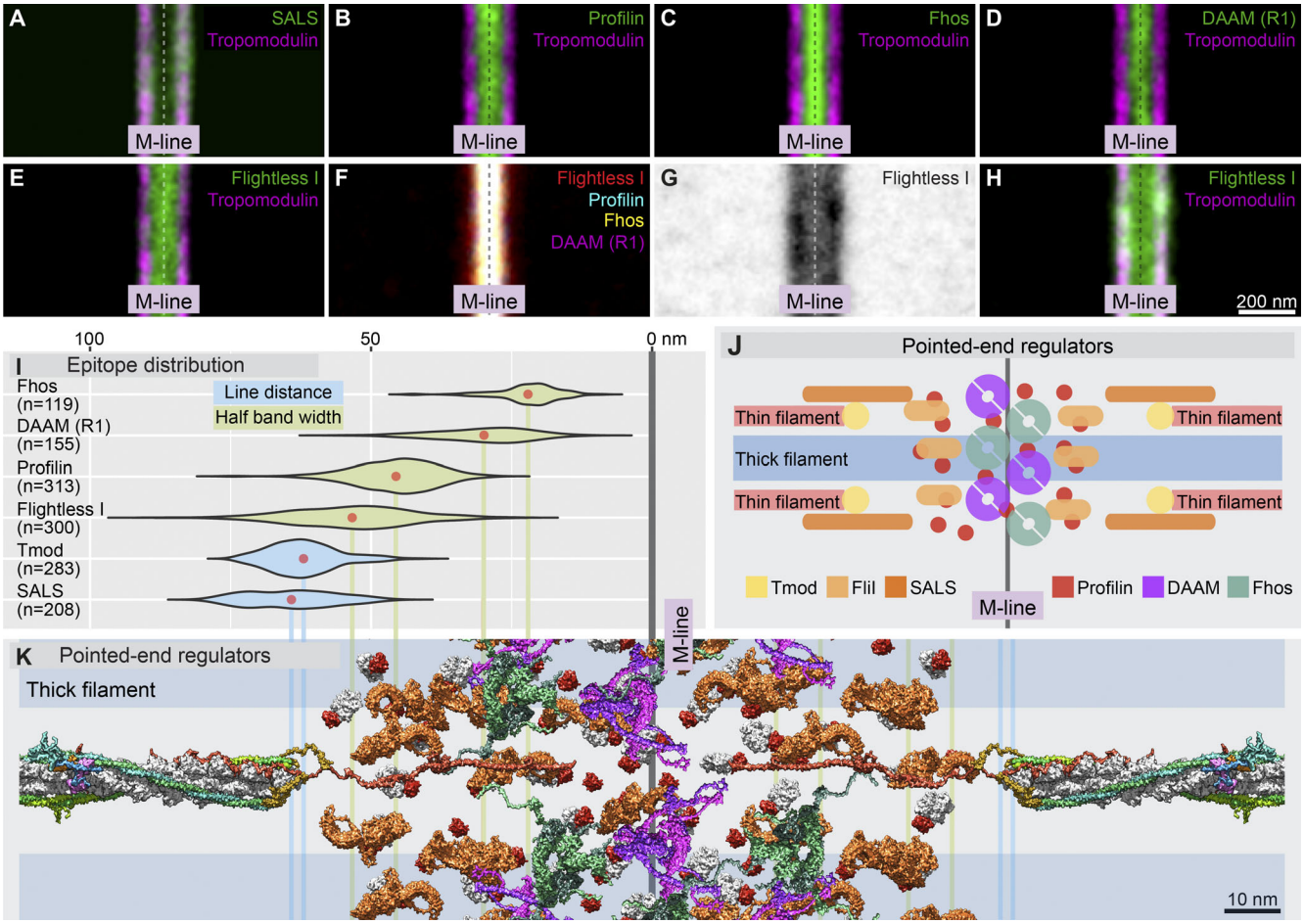

Figure 9. **Nanoscale arrangement of the actin regulatory proteins in the H-zone. (A–H)** Distribution of the actin-binding protein SALS, Profilin, Fhos, DAAM, and FliI as compared with the pointed-end–capping Tmod protein (A–E, G, and H) or each other (F). Scale bar, 200 nm. **(I)** Longitudinal epitope distributions relative to the M-line, depicted as violin plots. Plot color indicates the corresponding protein density class and the applied measurements. Mean values are shown as red dots. **(J)** Schematic arrangement of the actin regulatory proteins at the M-line. **(K)** Molecular model of actin regulatory protein distribution in the H-zone/M-line region, scaled to the plots in I, with vertical lines marking the average epitope positions. F-Actin is shown in gray, DAAM in magenta, Fhos in light green, Flightless in orange, Profilin in red, SALS in red orange, Tm in green, and Cpa in cyan. Scale bar, 10 nm.

the large Obscurin isoform by the small one (lacking the N-terminal domains of the large one) in mature flies (Katzemich et al., 2012) might be a novel mode of regulation of pointed end dynamics. Moreover, the refined nanoscopic arrangement of Obscurin also determines the position of its known interactors: Ball, which was identified as a ligand of the kinase1 domain, and MASK, a ligand of both kinase1 and kinase2 domains (Katzemich et al., 2015). In addition, Obscurin is likely to interact with Zormin, a potential functional homologue of the C-terminus of Titin. Interestingly, the Zormin double lines were close to our resolution limit, and for this reason, their separation is not evident on the averaged density image. Yet, this example clearly demonstrates that in terms of resolution, SMLM can outperform immuno-EM (Burkart et al., 2007) due to its superior labeling density.

One of the major unsolved questions of sarcomere development is the mechanism of thin filament assembly at the pointed end. Examination of the distribution of the thin filament elongation regulatory proteins in the H-zone led to the unexpected conclusion that these proteins localize into two distinct spatial domains. Notably, Tmod and SALS are localized directly at the pointed end, while the formins and associated factors are highly enriched in a narrow band in the middle of the H-zone. Together, these data suggest that the major place for actin assembly is not in the immediate vicinity of the pointed end rather in an M-line–centered narrow domain. Due to physical separation of the pointed ends from the actin assembly machinery, including the bulk of the polymerization-competent Profilin-G-actin pool, these results argue against models based on actin monomer incorporation at the pointed end, but support the possibility of formin-mediated (short) F-actin oligomer formation in the central zone that could subsequently fuse to the pointed ends under the control of Tmod and SALS. Thus, our localization studies provide solid ground for an F-actin annealing–based pointed-end elongation mechanism.

We believe that our approach and localization atlas together will be useful to a wider community and will pave the way for further mechanistic modeling of the sarcomere. Whereas this nanoscopic approach has proved very promising, it will be important to extend the scope of this analysis toward developmental

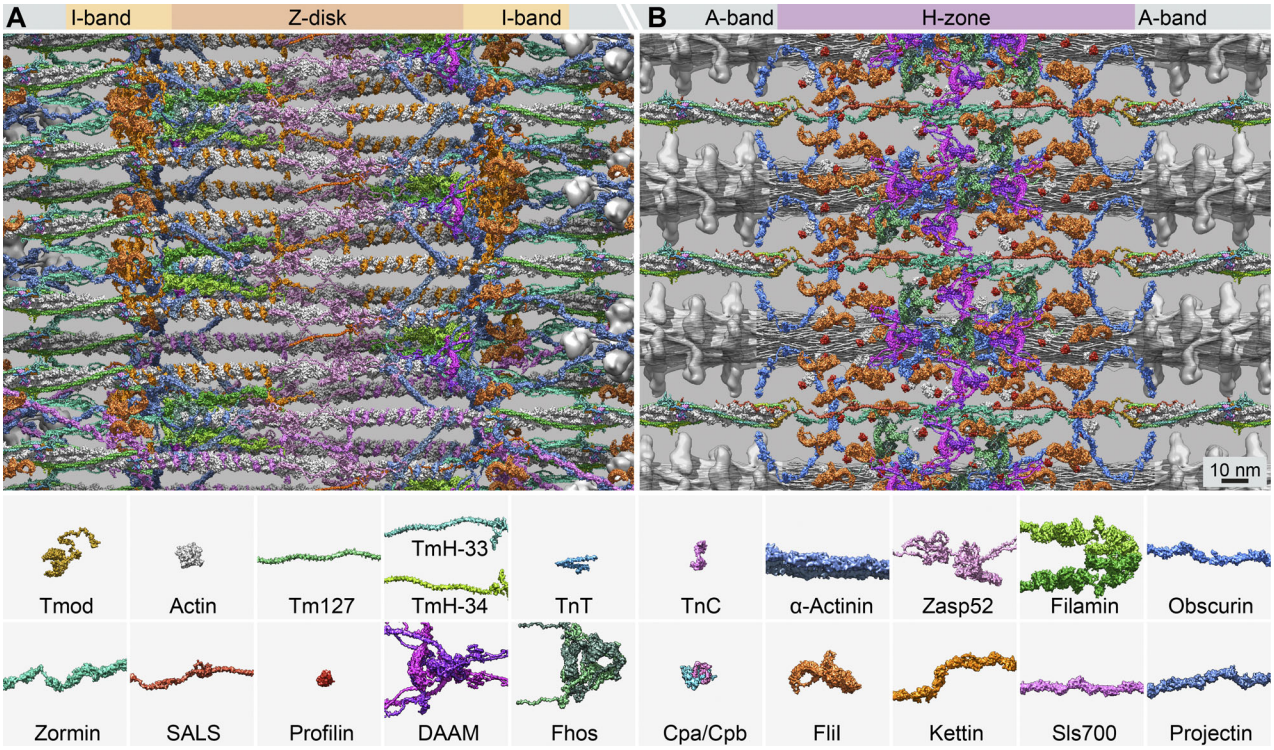

Figure 10. **Molecular model of the I-band and H-zone. (A and B)** A section through the I-band (A) and H-zone (B), indicating 25 proteins. Proteins are shown according to our template-based protein structure modeling and placed according to the localization data presented combined with the known lattice structure of the IFM. The graphical legend at the bottom indicates the different proteins. Scale bar, 10 nm.

and evolutionary directions. It will be interesting to map the protein distributions during the actively elongating phases of sarcomere assembly as well as in ageing muscles. Undoubtedly, the success of this analysis strictly relied on the exceptional regularity of the IFM sarcomeres; therefore, probing the evolutionary conservation of the fruit fly data in vertebrate striated muscle sarcomeres appears as an exciting future adventure.

Materials and methods

Drosophila stocks

Fly strains were raised under standard laboratory conditions at 25°C. As wild type, we used an isogenized w^{1118} strain. For aging, freshly hatched flies were collected and kept on fresh food until the desired age was reached. To test the association of DAAM with the filamental system, we used $Act88F^{KM88}$ mutants, which lack myofibrillar actin in the IFM (Hiromi and Hotta, 1985), and Mhc^{10} mutants (Collier et al., 1990), in which myofibrillar Myosin is absent.

Igase treatment

The proteolytic removal of the C-terminal extension of TmH-34 was performed as described previously (Clayton et al., 1998; Iwamoto, 2013). Briefly, the glycerinated fibers were incubated overnight (~12 h) at 4°C in a rigor solution containing endoproteinase Pro-Pro-Y-Pro (Igase; MoBiTec) prior fixation. The control fibers were incubated for the same period in the rigor solution without the endoproteinase.

Protein expression and purification

To test the specificity of the DAAM antibodies, Schneider 2 cells were transfected with a plasmid containing the CDS of either DAAM-PB or DAAM-PD. Expression clones were created by using standard Gateway LR reaction, where pENTR3C-DAAM-PB and pENTR3C-DAAM-PD were used as entry clones and pAWF served as a destination vector (Molnár et al., 2014). Total lysates of Schneider 2 cells were analyzed by Western blot using a pan-DAAM (R4, 1:1,000; Gombos et al., 2015) and a DAAM-PD–specific antibody (PD, 1:500). Cell transfection and lysis were performed as described elsewhere (Gombos et al., 2015).

To analyze the domain specificity of the DAAM antibodies (R1 and R4), FH1, FH2, and DAD-CT domains of DAAM were produced in *Escherichia coli* (BL21) as GST-tagged recombinant proteins using the pGex expression system. Protein purification was performed as described previously (Barkó et al., 2010). 200 ng of each recombinant protein was loaded onto an SDS-PAGE gel and analyzed by Western blot using the anti-R4 (1:5,000) and anti-R1 (1:5,000) DAAM antibodies. SDS-PAGE and Western blot were performed by using standard procedures. Anti-Rabbit-HRP (1:10,000; Jackson) secondary antibody and an ECL reagent (Millipore) were used to detect immunocomplexes.

Preparation of myofibrils for superresolution imaging

For SMLM, individual myofibrils were isolated from the IFM of anesthetized adult (~24 h after eclosion) *Drosophila* as described previously (Burkart et al., 2007), with minor modifications. In brief, bisected hemithoraces were incubated in relaxing solution

(100 mM NaCl, 20 mM NaPi, pH, 7.0, 5 mM $MgCl_2$, 5 mM EGTA, and 5 mM ATP) supplemented with 50% glycerol for 2 h at 4°C. Afterward the dorsal longitudinal muscles were isolated from the hemithoraces and dissociated by gently pipetting them in an Eppendorf tube in the presence of 0.5% Triton X-100. Dissociated myofibrils were centrifuged at 10,000 rpm for 2 min. Myofibrils were washed and centrifuged two more times in relaxing solution. Myofibrils were resuspended in relaxing solution, and 20 µl of the sample was dropped on a glass coverslip and fixed with 4% paraformaldehyde (Alfa Aesar) in relaxing solution for 15 min. After washing three times in relaxing solution, the samples were blocked in blocking solution (5% goat serum [Sigma] and 0.1% Triton X-100 in relaxing solution) for 30 min in a humidity chamber. Primary antibodies (see Table S1) were applied overnight at 4°C in blocking solution. Following washes, the appropriate Alexa Fluor 647–conjugated (1:600; Life Technologies) secondary antibodies were applied for 2 h at room temperature. The samples were thoroughly washed and stored in PBS prior to imaging.

Antibodies

The primary antibodies used in this study are listed in Table S1. Detection was achieved with goat anti-rabbit, anti-mouse, or anti-rat IgG highly cross-absorbed secondary antibodies coupled to Alexa Fluor 488, Alexa Fluor 546, or Alexa Fluor 647 (1:600; all from Life Technologies). F-Actin was labeled with either Alexa Fluor 488– or Alexa Fluor 546–phalloidin (1:200; Life Technologies). G-Actin was labeled with Alexa Fluor 488–deoxyribonuclease I (1:500; Thermo Fisher Scientific).

Antibody generation

The anti-DAAM-PD antibody was raised against an N-terminal polypeptide (INEPDTHSANTEILQTSP) corresponding to amino acid residues 26–43 of the DAAM-PD isoform, in a transgenic rabbit strain expressing the Fc receptor by ImmunoGenes Kft. Animals were immunized with 200 µg DAAM-PD-INEP peptide-KLH conjugate in complete Freund's adjuvant and challenged multiple times with 100 µg of the conjugate in incomplete Freund's adjuvant. Sera containing antibody to DAAM-PD were affinity purified with a SulfoLink Immobilization Kit for peptides (Thermo Fisher Scientific), according to the manufacturer's instructions.

Confocal laser scanning microscopy

Confocal images were captured on a Zeiss LSM880 microscope, equipped with a 40×, 1.4-NA oil-immersion lens. Images were acquired according to the Nyquist rate, using the complete dynamic range of the detectors. Brightness and contrast of the images were linearly adjusted in Fiji (National Institutes of Health). Samples were prepared as described above, except they were mounted in antifade reagent (ProLong Gold, P36930; Life Technologies) for imaging.

Superresolution SIM and STED imaging

SIM was performed on a Zeiss Elyra S1 SIM microscope with a Plan-Apochromat 63×/1.4-NA oil-immersion objective. STED microscopy was performed on a Leica TCS SP8 STED 3× microscope with a 100×/1.4-NA oil-immersion objective and HyD time-gated photodetectors. Acquired images were deconvolved with Huygens Professional (SVI) before analysis.

Superresolution dSTORM imaging

Superresolution dSTORM measurements were performed on a custom-made inverted microscope based on a Nikon Eclipse Ti-E frame. After being conditioned (through spatial filtering via fiber coupling and beam expansion), the applied laser beams were focused into the back focal plane of the microscope objective (CFI Apo 100×, 1.49 NA; Nikon), which produced a collimated beam on the sample. The angle of illumination was set through a tilting mirror mounted into a motorized gimbal holder and placed into the conjugate plane of the sample. All dSTORM images were captured under EPI illumination at an excitation wavelength of 647 nm (647 nm, P_{max} = 300 mW; MPB Communications). The laser intensity controlled via an acousto-optic tunable filter was set to 2–4 kW/cm^2 on the sample plane. An additional laser (405 nm, P_{max} = 60 mW; Nichia) was used for reactivation. Images were captured by an Andor iXon3 897 BV EMCCD digital camera (512 × 512 pixels with 16-µm pixel size). The size of the illuminated region of the sample was matched to the size of the detector, which determined the field of view (80 × 80 µm^2). Frame stacks for dSTORM superresolution imaging were typically captured at a reduced image size (crop mode). Two separate fluorescence filter sets (LF405/488/561/635-A-000 and Di03-R635-t1 dichroic mirrors with BLP01-647R-25 emission filters; Semrock) were used to select and separate the excitation and emission lights in the microscope. During the measurements, the perfect focus system of the microscope was used to keep the sample in focus with a precision of <30 nm. Right before the measurement, the storage buffer of the sample was replaced with a GLOX switching buffer (van de Linde et al., 2011) and the sample was mounted onto a microscope slide. Typically 20,000–50,000 frames were captured with an exposure time of 20 or 30 ms.

Single-molecule localization

The captured and stored image stacks were evaluated and analyzed with rainSTORM localization software (Rees et al., 2013). Individual images of single molecules were fitted with a Gaussian point spread function (PSF), and their center positions were associated with the position of the fluorescent molecule. Localizations were filtered via their intensity, precision, and SD values. Only localizations with precisions of <20 nm and SD between 0.8 and 1.0 were used to form the final image and for further analysis. In our system, the focused PSFs have a σ size of ∼0.9. The strict PSF filtering was applied in order to discard the majority of the overlapping blinking events. Mechanical drift introduced by either the mechanical movement of the sample or thermal effects was analyzed and reduced by means of a correlation-based blind drift correction algorithm. Spatial coordinates of the localized events were stored, and the final superresolved image was visualized with a pixel size of 10 nm.

Experimental pipeline and quantitative measurements

To achieve reliable measurements, we repeated every staining experiment independently at least three times, with myofibrils

isolated from at least 20 *white*^{1118} females. For each antibody, we acquired dSTORM images from numerous (on average >200) sarcomeres. Based on their distribution along the myofibril longitudinal axis, we classified epitope images at the H zone and/or the I-band into the following categories: double lines, bands, or gaps. Quantitative measurements were performed in several steps after filtering the raw dataset for Thompson precision (<20 nm) and PSF size ($0.8 \le \sigma \le 1.0$).

Step 1: Classification and segmentation

A square-shaped area around the studied structure (double line, band, or gap) is segmented manually in rainSTORM (rainSTORM software and manual are available at http://titan.physx.u-szeged.hu/~adoptim/?page_id=582) using the "Export box section" tool. Localizations inside this selected area are only analyzed further using the IFM Analyser tool (IFM Analyzer software and manual are available at http://titan.physx.u-szeged.hu/~adoptim/?page_id=1246).

Step 2: Initial region of interest assignment

A straight line is coarsely fitted on the coordinates of the localizations inside the selected area. The center coordinates of all the localizations and the straight-line orientation are used to define the position and orientation of a smaller rectangle (typically set to 600 × 800 nm) within which a further subset of localizations were cut out for quantitative evaluation. The rectangle can further be adjusted manually if necessary. The size of this area is matched to the target feature: it is set approximately three to four times broader and 10% shorter than the actual structure to clearly separate it from its background and eliminate edge artifacts.

Step 3: Central curve fitting

The symmetry axis of the structure is determined more precisely via a second-order polynomial fit, taking into consideration the curvature of the selected structure. To achieve this fit, a Gaussian kernel is applied on the localizations to get a smoothed localization density map. The kernel size was chosen to be large enough to effectively blur the localizations but small enough to preserve the gap or the double-line structures (~20 nm). A polynomial was then fitted along the minima (in case of double lines and gaps) or along the maxima (in case of single bands) of the localization density and was considered as the symmetry axis of the structure.

Step 4: Emitter distribution and initial fitting

Following that, the distance of each localized point from the fitted symmetry axis is determined numerically and depicted in a histogram. The acquired histogram shows the localization distribution rather than the epitope/binding site distribution, which is closely related to the protein distribution. This discrepancy arises for two main reasons: localization precision and linker length. Localization precision is determined by the localization algorithm based on the characteristics of the blinking event. Theoretically, the fluorophore distribution can be calculated by deconvolving the measured localization image with the localization precision distribution (which can typically be described by a Gaussian curve). The epitope distribution can be obtained from the fluorophore distribution and the length of the linker. We assume that the fluorophores are distributed evenly on a sphere around the epitope at a radius equivalent to the linker length (the size of the primary and secondary antibodies is ~20 nm).

Step 5: Epitope distribution

To quantitatively characterize the epitope distributions, a theoretical curve, in which the aforementioned effects are considered, is calculated and fitted to the measured data. During this process, we approximate the epitope distribution of the band, the double line, and the gap structures with a single Gaussian, double Gaussians, and negative top-hat functions with additional peaks at the edges, respectively. Then, the approximated epitope distribution is smeared with the linker and with the average Thompson precision using convolution. The resultant distribution is compared with the measured histogram, and the fitting algorithm varies the epitope distribution parameters until good agreement is met. From the fitted parameters, the values quantitatively describing the double line, band, and gap structures can be extracted in a straightforward manner.

Analysis of the geometric parameters of subsarcomeric structures

Double lines

A significant fraction of the antibodies displayed a double-line-type distribution along the symmetry axes of the H-zones and/or I-bands with characteristic line distances. In these cases, the longitudinal density distributions can be approximated with a double Gaussian, where the peak centroids represent the average epitope position. We used the line distance parameter (M- or Z-line distance) to describe the distance between the midline of the H-zone/I-band and the fitted peak centroid. We consider these measurements to be the most reliable ones, as the Gaussian distributions are sensible estimates of the emitter distribution and their centroid positions are independent (within reasonable limits) of the localization precision and the labeling density or length of the linkers (the size of the primary and secondary antibodies).

Bands

Some of the antibodies labeled the midline of the H-zone or I-band. This localization pattern could correspond to (1) a real band-type epitope distribution around the symmetry axes or (2) a hidden double-line-type distribution, where the resolution is not sufficient to resolve individual "lines." Unless indicated otherwise, we presumed the first scenario. Since bands are settled on the symmetry axes, their peak position is self-evident; therefore, we quantified their thickness, which is characteristic to each antibody/epitope. The localization distribution of bands can be best approximated with a Gaussian distribution, but their apparent width is an overestimation of the real value, since linker length and localization precision alter the extent of the localizations in an additive way. Nevertheless, the IFM Analyser accounts for these effects and generates an estimated epitope distribution profile. We measured the full width at half maximum of these epitope distribution profiles and used the half-bandwidth values to describe them. ZASP52 in the Z-disk and

FliI in the H-zone presented in two forms; some classify as double lines and the rest clearly as bands. We presume that the observed bands are actually double-line structures that we cannot resolve. However, we can estimate the line distances in these instances by performing band-type measurements on the double-line structures. We found that the band widths (full width at half maximum) were consistently 1.6–1.7 times larger than the line distances measured on the same structures. We used the average value of 0.615 as a conversion unit to estimate the line distances from the bandwidth measurements in these cases. We also assumed hidden double-line structures in the case of Obscurin (Ig14–16), Obscurin (Kin1), and FLN N-terminal epitopes and used the same method to estimate the line distances.

Gaps

The antibodies that labeled the A-band (more or less uniformly) formed clear gaps in the H-zone and/or I-band. These gaps are located precisely on the symmetry axes, and their widths are informative. However, the apparent widths, based on localization distribution, are an underestimation of the real values for the aforementioned reasons. To obtain more realistic approximations, the primary fitted distribution profile was convolved as previously. We used the half gap width to characterize the epitope distribution in these cases.

Visualization

Quantitative measurements were performed on individual structures, but for visualization purposes, we used the IFM Analyser to align the localizations along the symmetry axes of the H-zone/I-band before averaging them. From the merged event lists a superresolved image was generated using the Simple Histogram method from rainSTORM. The averaged images gave thorough representation of the longitudinal and transverse distributions of the individual protein targets. Relying on the symmetry axes of the H-zone and I-band, we aligned independently averaged protein densities to generate pseudo-multicolor representations.

Template-based protein structure modeling and constructing the molecular representation of the H-zone and I-band

To build the molecular structure of the IFM, we used coordinates from the PDB and maps from the Electron Microscopy Data Bank, if they were available. In the absence of PDB data, structural information was generated by template-based modeling using the RaptorX server (Källberg et al., 2012) and annotated protein sequences from FlyBase. Graphical models of selected proteins were generated in UCSF Chimera (Pettersen et al., 2004), and scaled images were exported in an orthographic projection. Although RaptorX is a leading prediction server, based on the assessment of weekly prerelease PDB sequences, some uncertainties in our contour length estimations cannot be strictly excluded. Separate models are combined in Illustrator (Adobe) and arranged to be consistent with our measurements and the 3D lattice structure of *Drosophila* IFM filaments (Vigoreaux, 2007). As to stoichiometry of the muscle proteins, published data allow quite precise estimations for all the major thin filament components, and the ratio of actin filaments versus thick filaments is also known. In case of FLN, α-Actinin, and to some extent elastic filaments, available biochemical, EM, and genetic data provide us with a reasonably good estimation, whereas for most other proteins, the current literature is not informative in this regard. Thus, we note that with the exceptions of the basic thin and thick filament backbones, our models are limited in terms of stoichiometry. Despite this limitation at the global scale, the models built are important to visualize the potential protein–protein interactions and key structural arrangements on a smaller scale.

Thin filament model

To generate a thin filament model, we used the previously established quasiatomic IFM thin filament structure (PDB: 2W49; Wu et al., 2010) as a backbone.

Of the two Tmod isoforms (Mardahl-Dumesnil and Fowler, 2001), the larger is the dominant isoform in mature (>24-h adults) IFM, and this was used in our model. The tertiary structure of Tmod-PB is based on the previously characterized Tmod-pointed-end structure (PDB: 4PKG, 4PKH, and 4PKI; Rao et al., 2014).

There are three Tm isoforms in the IFM: the standard striated muscle Tm127 isoform and two IFM-specific heavy Tms, TmH-33 and TmH-34. For simplicity, we used an identical structure to depict the Pro-Ala–rich C-terminal extensions of the two heavy Tms. The N-termini of Tm are oriented toward the pointed end, and we confirmed this orientation using the MAC141 antibody, the epitope of which has been narrowed down to an 80-aa sequence at the N-terminus (Cho et al., 2016). Alignment of the relevant N-terminal sequences of all Tm isoforms thought to be recognized by MAC141 reveals a common sequence motif of 12 aa long at the very N-terminus of these proteins (Fig. S2 A). Given that rest of the region does not contain conserved sequences that would be sufficiently long as antigens, it appears very likely that the MAC141 epitope is located within the extreme N-terminal 12 aa. A peculiar feature of the MAC141 staining is evident in a difference between the I-band and H-zone patterns. Notably, in the I-band, we found a gap-type distribution, whereas in the H-zone, the double lines appear to consist of two discrete peaks each, based on the distribution of the measurements. The epitope position in the I-band is entirely consistent with an N-terminal location. In case of the H-zone double peaks, the M-ward one perfectly overlaps with the pointed ends corresponding to the expected position, while the other peak is in the middle of the most proximal axial repeat. By combining it with the Igase treatment data and assuming that the most proximal Tn complex is missing from some of the thin filaments/myofibrils, the second peak corresponds to the average position of the two most M-ward epitopes. Interpretation of the MAC143 epitope position that labels the C-terminus of the TmH-34 (Fig. 3, C, F, I, and J) is not trivial, since it is known to recognize an additional thin filament component, GstS1 (Clayton et al., 1998). Nevertheless, our localization data suggest that the TmHs are not part of the most Z-ward Tm repeat.

The regulatory heterotrimeric Tn complex, composed of TnT, TnC, and TnI, is attached to the Tm dimers. Former EM and

structural studies (Wendt et al., 1997; Wendt and Leonard, 1999) demonstrated that the Tn core complex in the *Lethocerus* IFM is located on the Tm overlap. However, the position of the Tn complex with respect to the N- and C-termini of Tm could not be determined from EM images. The anti-TnC staining gave a double-line-type distribution in the I-band with a Z-line distance of 65 nm (Fig. 2, E, F, and I), which clearly positions it to the C-terminus of the most Z-ward Tm repeat. Similarly to Tm, the accessibility of TnC antibody (Qiu et al., 2003) is limited in the A-band. Our TnT measurements indicate that in the I-band, it binds the C-terminal part of Tm. However, in the H-zone, the measured average position is somewhat (∼14 nm) more Z-ward than expected. One possible explanation is that the Tn complex is missing from some of the most M-ward repeats at the pointed end. This scenario would explain the relatively large SD measured at the H-zone, and it could account for a shift in the position toward the barbed end.

Z-disk model

We generated an approximate IFM lattice structure based on the ultrastructural analysis performed on the Z-disk of *Apis mellifera* (Cheng and Deatherage, 1989; Deatherage et al., 1989; Rusu et al., 2017). The lattice spacing between filaments in the Z-disk is altered as the filaments in groups of three get closer to the edge of the Z-disk. Thick filaments are placed such that they project to the trigonal position of the three thin filaments.

In the IFM, a 104-kD muscle-specific α-Actinin isoform (Actn-PB) is expressed. The epitope recognized by the α-Actinin antibody is unknown. Because the α-Actinin dimer is smaller (∼36 nm) in length than the optical resolution of our system, we cannot resolve the individual epitopes independently within the dimers. Since they form a symmetric antiparallel structure (Djinović-Carugo et al., 1999), the emitter peak positions should mark the centroid of the dimers, regardless of the exact epitope position and orientation of the dimer (by assuming an isotropic emitter distribution). It is thought that the exact position, angle, and polarity of α-Actinin binding are governed by extrinsic factors. In vertebrates, the 19-nm periodicity of α-Actinin might be regulated by Nebulin/Nebulette proteins and/or the number of Z-repeats within the N-terminus of Titin, which are both expressed differentially in different muscle types (Gautel et al., 1996). However, the corresponding proteins are missing or quite different in *Drosophila*; instead, Zasp52 was shown to be required for the association of α-Actinin with the Z-disk (Chechenova et al., 2013). In *Drosophila*, Zasp52 is the major member of the Alp/Enigma family of PDZ-LIM domain proteins. Many different Zasp52 splice isoforms have been identified, resulting in up to 61 different proteins, some of which are restricted to specific muscle types (Katzemich et al., 2011). We used the Zasp52-PF isoform in our model as a representative of one of the annotated adult-specific isoforms (including the large exon 16) recognized by the Z(210) monoclonal antibody (Saide et al., 1989).

FLN, encoded by *cher* in *Drosophila*, is known as an actin filament cross-linking protein. It has ≥10 different transcript isoforms, and most of them are expressed in the IFM. We used Cher-PM in our model as a representative of one of the large isoforms (group D; Gonzalez-Morales et al., 2017). FLM in our model is located in the trigonal position of the Z-disk thin filaments facing a thick filament.

Thick filament model

A 3D structure of the IFM thick filaments (from *Lethocerus*) has recently been reported with a resolution of ∼5.5–20 Å (EMDataBank accession code EMD-3301; Hu et al., 2016, 2017). Since the Myosin II sequence homology among insects is extremely high, we relied on this reconstruction in our model. While it provides remarkable structural insights regarding the bridge region (A-band), it does not represent the central, head-free bare zone or the tapered ends of the filament. Consequently, we used a simplified representation of these regions in our model. In the insect flight muscle, size of the S2 segment has been determined by EM-tomography–based structural studies as being ∼11 nm, and it was also revealed that the S2 segment practically overlaps with the S1 region (head of Myosin) along the longitudinal axis of Myosin (Liu et al., 2006). The M-line gap distance (73.9 nm) measured by dSTORM in the IFM suggests an arrangement similar to the vertebrate M-line. In vertebrates, the M-line distance of the most proximal (P1 and P1′) crown level is 77 nm (Al-Khayat et al., 2010), which is also plausible in the IFM, since from our measurements it would perfectly position the P1 and P1′ crown level to the most M-ward target zone on the thin filaments.

In the *Drosophila* IFM, while the thin filaments are in perfect register, the thick filaments form a "superlattice" with a 4.83-nm axial shift between adjacent thick filaments along a MyAc layer (Squire et al., 2006), which is accounted for in our modeling.

Modeling of the H-zone backbone

The myofilament lattice arrangement has been measured very accurately, resulting in a center-to-center thick filament spacing of 56.0 nm (Chan and Dickinson, 1996), and it is known that the IFM contains thin to thick filaments in a ratio of 3:1. Based on this information, a 3D A-band lattice structure can be assembled, although on most figures we used a 2D MyAc layer representation.

In the IFM of young adult flies, the ∼475-kD Obscurin A (unc-89-PC) isoform is present. In building a detailed model of the H-zone complex, we considered additional potential constrains: (1) Obscurin is able to form assemblies independent of Myosin, which suggests that it is cross-linked either directly or indirectly and ready to incorporate Myosin to form a hexagonal superlattice; (2) it forms a complex with Myosin (Katzemich et al., 2012); the (3) the Obscurin epitope recognized by the Ig14–16 antibody is confined to a small area close to the thick filaments based on immuno-EM (Katzemich et al., 2012); and (4) Obscurin almost certainly interacts with Zormin (discussed below).

The vertebrate H-zone contains the C-terminus of Titin, which can bind Myomesin and Obscurin. However, in *Drosophila*, Titin is replaced by the smaller proteins of Sls and Projectin (Bullard et al., 2005). Of these, only the Sls isoform Zormin has been found in the H-zone (as well as in the I-band; Burkart et al., 2007). There are two Zormin isoforms in the IFM, but in the absence of information, regarding their isoform

distribution, we used the sole Zormin-PE isoform in our model. In vitro the Zormin Ig4–6 domains can bind both Myosin and actin (Burkart et al., 2007), but in vivo, the H-zone localization of Zormin depends on Obscurin (Katzemich et al., 2012). There is no available information on whether Zormin crosses over between thin filaments or is arranged in a strictly parallel fashion, but mechanical considerations (Agarkova and Perriard, 2005) make a cross-linking Zormin arrangement more plausible.

Modeling of the thin filament regulators

SALS (Sals-PB) can bind both F- and G-actin in vitro (Bai et al., 2007), but in diffraction-limited images, it was not possible to determine whether its in vivo association with the thin filament is direct or indirect. Considering its size (~150 kD) and localization in the H-zone, a physical interaction between SALS and the pointed end/Tmod is highly probable. In the I-band, the SALS epitopes are positioned next to the formins on the barbed ends. However, SALS was shown to cosediment with Gelsolin-capped F-actin, leading to the conclusion that SALS interacts with F-actin through pointed ends or side binding, but not through the barbed ends (Bai et al., 2007). Nevertheless, since Gelsolin is not an effective barbed-end capper (Rao et al., 2014), we would not exclude the possibility that SALS is in fact able to bind the barbed ends.

Since the C4 antibody gives a sparse signal along the entire myofibril, including the H-zone, we presume the presence of monomeric actin in the H-zone, which is also supported by our DNaseI staining (Mannherz et al., 1980). Therefore, some of the Profilin molecules (Chic-PA; Verheyen and Cooley, 1994) are depicted in a G-actin–bound form in our model (PDB: 3U4L).

Of the two formins examined, *Fhos*, the single *Drosophila* FHOD subfamily orthologue, expresses two protein isoforms in the IFM (Shwartz et al., 2016): a short Fhos-PA isoform that localizes to the H-zone and a large Fhos-PH isoform enriched in the I-band (Shwartz et al., 2016). Similarly to *Fhos*, the sole *Drosophila DAAM* orthologue also expresses a short and large IFM isoform called DAAM-PB and DAAM-PD, respectively. However, the sarcomeric distribution of the short and large isoforms has not yet been clarified. While the antibody recognizing both isoforms (R1; Matusek et al., 2006) displayed an H-zone and I-band localization, the PD isoform–specific antibody exclusively localized to the I-band. In conclusion, both formins have the same isoform distribution; i.e., the short isoforms are located in the H-zone and the large isoforms are located in the I-band.

FliI (FliI-PA) is a conserved member of the Gelsolin family and essential for early development both in vertebrates and *Drosophila* (Campbell et al., 1993). In the IFM, FliI localization partially overlaps with the short formin isoforms and almost completely colocalizes with Profilin. Since FliI contains six Gelsolin-like repeats, it presumably interacts with Profilin-actin.

Modeling of the elastic filaments

Sls is a large modular protein similar to the I-band region of vertebrate Titin. It has four IFM isoforms, including two Zormin isoforms with predicted sizes of 324 kD and 388 kD, the 527-kD Kettin (Sls-PA), which is the most abundant Sls isoform, and a minor amount of the 724-kD Sls(700) (Burkart et al., 2007). Kettin, the major Sls isoform in the IFM, is composed of 35 Ig domains separated by linker sequences. Previous immunoelectron micrographs show that the Ig3 domain is positioned approximately in the middle of the Z-disk (Kulke et al., 2001), while the average Z-line distances of Ig16 and Ig24 are ~50 nm and ~60 nm (Kulke et al., 2001), respectively. Remarkably, our measurement for Ig16 is 49.2 nm (nearly identical to the 50 nm measured by EM), whereas the Z-line distance if Ig35 is 66.8 nm, which is a position ~35 nm away from the edge of the A-band. The N-terminally located region 1 of Kettin, which contains a unique sequence motif and four Ig domains (Ig1–Ig4) with variable linker lengths, is unlikely to bind actin (Hakeda et al., 2000). Nevertheless, this region might be involved in a head-to-head interaction with another Kettin molecule (Hakeda et al., 2000) and/or interacts with other Z-disk proteins. The dimerization of Kettin is supported by the fact that, in vitro, it promotes the antiparallel association of actin filaments (van Straaten et al., 1999). This suggests that either one Kettin molecule binds two antiparallel actin filaments or that Kettin molecules dimerize in an antiparallel way. While available data do not provide direct support the first hypothesis, our modeling approach favors the second one. Ig domains 5–20 in region 2 are separated by linkers of almost constant length, and using this central region of Kettin, it was demonstrated that the Ig domains with their linkers are able to bind actin with a stoichiometry of one to one (van Straaten et al., 1999). Also, the approximate distance between Ig3 and Ig16 suggests that this region binds actin by following the F-actin short pitch helix, as Ig3 has been positioned to the center of the Z-disk (van Straaten et al., 1999). In region 3 (Ig21–Ig31), the linkers are slightly variable in length, and the previously measured distance between Ig16 and Ig24 (~10 nm) suggests that it is not binding actin in the same way as it does in region 2. Finally, region 4 is separated from the other regions by a long linker and possesses four Ig domains (Ig32–Ig35) and relatively short spacers. Taken together, these data prompted us to revisit the structural arrangement of Kettin. Because we measured the distance of Ig16 to Ig34 as ~18 nm, which should be at least 72 nm in a fully extended molecule model, we interpret this result as indication for a bunched structure. In addition, position of the most C-terminal Kettin domains is almost identical to the position of the Ig24 domain, which also supports the existence of a globular structure right next to the most Z-ward Tn complex. Interestingly, this structure might be identical to the electron-dense blobs identified on the thin filaments (Trombitás and Granzier, 1997) from which the connecting strands emerge toward the thick filaments.

The connecting protein Projectin is detected in the I-band. The Bt-PF isoform we worked with is composed of repeated Ig and Fn motifs and can be divided into five subregions: N-terminal, core, intermediate, kinase, and C-terminal regions (Ayme-Southgate et al., 2005). The N-terminal region is composed of two blocks of Ig domains separated by an extensible PEVK-like region. Based on immunoelectron micrographs (NT-1 antibody), the N-terminal region is located within the Z-disk (Ayme-Southgate et al., 2005). The P5 antibody has also been suggested to recognize an N-terminal epitope (Ayme-Southgate et al., 2005), but surprisingly, the average Z-line peak distance

measured by dSTORM is 74.9 nm, which positions it to the middle of the region between the Z-disk and the edge of the A-band. The N-terminal region is followed by the core region, which is composed of Fn-Fn-Ig modules repeated 14 times. We used a monoclonal antibody to determine the position of the Ig26 domain, which falls into this region and is thought to be anchored to the thin filaments (Kulke et al., 2001). It is 12 nm closer to the Z-line than the epitope recognized by the P5 antibody. Based on these measurements, we conclude that the P5 epitope is further toward the C-terminus than Ig26. After a short intermediate region, there is a kinase domain followed by five Ig domains at the C-terminus. The 3b11 antibody, which was raised against the C-terminus, is clearly located within the A-band (Ayme-Southgate et al., 2005).

Data analysis and figures

Data analysis was performed using custom analysis software, IFM Analyser, which was developed in MATLAB R2018b (MathWorks). Violin plots were generated using RStudio (RStudio Team, 2015). Figures were constructed in Illustrator CS6 (Adobe).

Online supplemental material

Fig. S1 shows the comparison of superresolution and sample preparation approaches. Fig. S2 shows the position and distribution of the Tm (MAC141) epitope. Fig. S3 shows the short and long isoforms of DAAM and the sarcomeric localization of Profilin and G-actin; it also shows that sarcomere association of DAAM depends on Mhc. Table S1 shows the primary antibodies used in this study. The supplemental figure PDF shows an overview of the structure and distribution of the imaged sarcomeric proteins.

Acknowledgments

We thank Velia Fowler (The Scripps Research Institute, La Jolla, CA), Belinda Bullard (University of York, York, UK), Florence Janody (Instituto Gulbenkian de Ciência, Oeiras, Portugal), Ben-Zion Shilo (Weizmann Institute of Science, Rehovot, Israel), Thomas Hays (University of Minnesota Twin Cities, Minneapolis, MN), Mirka Uhlirova (University of Cologne, Cologne, Germany), Norbert Perrimon (Harvard Medical School, Boston, MA), the Developmental Studies Hybridoma Bank, and the Bloomington *Drosophila* Stock Center for antibodies and fly stocks. We also thank Edina Szabó-Meleg for the help with SIM imaging. We are grateful to the European Molecular Biology Laboratory's Advanced Light Microscopy Facility for their support, in particular Imre Gáspár and Marko Lampe, for their help with STED and ground state depletion microscopy followed by individual molecule return imaging. We are indebted to John Sparrow, László Nyitray, and Miklós Erdélyi for critical reading and helpful comments on the manuscript. We thank Elvira Czvik, Anikó Berente, and Anna Rehák for technical assistance.

This work was supported by the Hungarian Science Foundation (K109330 to J. Mihály), the Hungarian Brain Research Program (KTIA_NAP_13-2-2014-0007 and 2017-1.2.1-NKP-2017-00002 to J. Mihály), the National Research, Development and Innovation Office (GINOP-2.3.2-15-2016-00001 and GINOP-2.3.2-15-2016-00032 to J. Mihály and GINOP-2.3.2-15-2016-00036 to M. Erdélyi), and Hungarian Science Foundation postdoctoral fellowships (PD 128623 to S. Szikora and PD 128357 to I. Földi).

The authors declare no competing financial interests.

Author contributions: Conceptualization, S. Szikora, M. Erdélyi, and J. Mihály; Methodology, S. Szikora, T. Gajdos, T. Novák, and M. Erdélyi; Investigation, S. Szikora, T. Gajdos, D. Farkas, and I. Földi; Software, T. Gajdos, T. Novák, and M. Erdélyi; Writing – Original Draft, S. Szikora, M. Erdélyi, and J. Mihály.; Writing – Review & Editing, S. Szikora, M. Erdélyi, P. Lenart, and J. Mihály; Visualization, S. Szikora and T. Novák; Supervision, M. Erdélyi, P. Lenart, and J. Mihály; Project administration, J. Mihály; Funding Acquisition, M. Erdélyi and J. Mihály.

Submitted: 4 July 2019
Revised: 4 October 2019
Accepted: 22 October 2019

References

Agarkova, I., and J.C. Perriard. 2005. The M-band: an elastic web that crosslinks thick filaments in the center of the sarcomere. *Trends Cell Biol.* 15:477–485. https://doi.org/10.1016/j.tcb.2005.07.001

Al-Khayat, H.A., R.W. Kensler, E.P. Morris, and J.M. Squire. 2010. Three-dimensional structure of the M-region (bare zone) of vertebrate striated muscle myosin filaments by single-particle analysis. *J. Mol. Biol.* 403:763–776. https://doi.org/10.1016/j.jmb.2010.09.025

Amândio, A.R., P. Gaspar, J.L. Whited, and F. Janody. 2014. Subunits of the Drosophila actin-capping protein heterodimer regulate each other at multiple levels. *PLoS One.* 9:e96326. https://doi.org/10.1371/journal.pone.0096326

Ayme-Southgate, A., J. Saide, R. Southgate, C. Bounaix, A. Cammarato, S. Patel, and C. Wussler. 2005. In indirect flight muscles Drosophila projectin has a short PEVK domain, and its NH2-terminus is embedded at the Z-band. *J. Muscle Res. Cell Motil.* 26:467–477. https://doi.org/10.1007/s10974-005-9031-8

Bai, J., J.H. Hartwig, and N. Perrimon. 2007. SALS, a WH2-domain-containing protein, promotes sarcomeric actin filament elongation from pointed ends during Drosophila muscle growth. *Dev. Cell.* 13:828–842. https://doi.org/10.1016/j.devcel.2007.10.003

Barkó, S., B. Bugyi, M.-F. Carlier, R. Gombos, T. Matusek, J. Mihály, and M. Nyitrai. 2010. Characterization of the biochemical properties and biological function of the formin homology domains of Drosophila DAAM. *J. Biol. Chem.* 285:13154–13169. https://doi.org/10.1074/jbc.M109.093914

Betzig, E., G.H. Patterson, R. Sougrat, O.W. Lindwasser, S. Olenych, J.S. Bonifacino, M.W. Davidson, J. Lippincott-Schwartz, and H.F. Hess. 2006. Imaging intracellular fluorescent proteins at nanometer resolution. *Science.* 313:1642–1645. https://doi.org/10.1126/science.1127344

Bullard, B., K. Leonard, A. Larkins, G. Butcher, C. Karlik, and E. Fyrberg. 1988. Troponin of asynchronous flight muscle. *J. Mol. Biol.* 204:621–637. https://doi.org/10.1016/0022-2836(88)90360-9

Bullard, B., C. Burkart, S. Labeit, and K. Leonard. 2005. The function of elastic proteins in the oscillatory contraction of insect flight muscle. *J. Muscle Res. Cell Motil.* 26:479–485. https://doi.org/10.1007/s10974-005-9032-7

Bullard, B., T. Garcia, V. Benes, M.C. Leake, W.A. Linke, and A.F. Oberhauser. 2006. The molecular elasticity of the insect flight muscle proteins projectin and kettin. *Proc. Natl. Acad. Sci. USA.* 103:4451–4456. https://doi.org/10.1073/pnas.0509016103

Burkart, C., F. Qiu, S. Brendel, V. Benes, P. Hååg, S. Labeit, K. Leonard, and B. Bullard. 2007. Modular proteins from the Drosophila sallimus (sls) gene and their expression in muscles with different extensibility. *J. Mol. Biol.* 367:953–969. https://doi.org/10.1016/j.jmb.2007.01.059

Campbell, H.D., T. Schimansky, C. Claudianos, N. Ozsarac, A.B. Kasprzak, J.N. Cotsell, I.G. Young, H.G. de Couet, and G.L. Miklos. 1993. The Drosophila melanogaster flightless-I gene involved in gastrulation and muscle

degeneration encodes gelsolin-like and leucine-rich repeat domains and is conserved in Caenorhabditis elegans and humans. *Proc. Natl. Acad. Sci. USA.* 90:11386–11390. https://doi.org/10.1073/pnas.90.23.11386

Chan, W.P., and M.H. Dickinson. 1996. In vivo length oscillations of indirect flight muscles in the fruit fly Drosophila virilis. *J. Exp. Biol.* 199: 2767–2774.

Chechenova, M.B., A.L. Bryantsev, and R.M. Cripps. 2013. The Drosophila Z-disc protein Z(210) is an adult muscle isoform of Zasp52, which is required for normal myofibril organization in indirect flight muscles. *J. Biol. Chem.* 288:3718–3726. https://doi.org/10.1074/jbc.M112.401794

Cheng, N.Q., and J.F. Deatherage. 1989. Three-dimensional reconstruction of the Z disk of sectioned bee flight muscle. *J. Cell Biol.* 108:1761–1774. https://doi.org/10.1083/jcb.108.5.1761

Cho, A., M. Kato, T. Whitwam, J.H. Kim, and D.J. Montell. 2016. An Atypical Tropomyosin in Drosophila with Intermediate Filament-like Properties. *Cell Reports.* 16:928–938. https://doi.org/10.1016/j.celrep.2016.06.054

Clayton, J.D., R.M. Cripps, J.C. Sparrow, and B. Bullard. 1998. Interaction of troponin-H and glutathione S-transferase-2 in the indirect flight muscles of Drosophila melanogaster. *J. Muscle Res. Cell Motil.* 19:117–127. https://doi.org/10.1023/A:1005304527563

Collier, V.L., W.A. Kronert, P.T. O'Donnell, K.A. Edwards, and S.I. Bernstein. 1990. Alternative myosin hinge regions are utilized in a tissue-specific fashion that correlates with muscle contraction speed. *Genes Dev.* 4: 885–895. https://doi.org/10.1101/gad.4.6.885

Deatherage, J.F., N.Q. Cheng, and B. Bullard. 1989. Arrangement of filaments and cross-links in the bee flight muscle Z disk by image analysis of oblique sections. *J. Cell Biol.* 108:1775–1782. https://doi.org/10.1083/jcb.108.5.1775

Djinović-Carugo, K., P. Young, M. Gautel, and M. Saraste. 1999. Structure of the alpha-actinin rod: molecular basis for cross-linking of actin filaments. *Cell.* 98:537–546. https://doi.org/10.1016/S0092-8674(00)81981-9

Fyrberg, E., C.C. Fyrberg, C. Beall, and D.L. Saville. 1990. Drosophila melanogaster troponin-T mutations engender three distinct syndromes of myofibrillar abnormalities. *J. Mol. Biol.* 216:657–675. https://doi.org/10.1016/0022-2836(90)90390-8

Gautel, M., and K. Djinović-Carugo. 2016. The sarcomeric cytoskeleton: from molecules to motion. *J. Exp. Biol.* 219:135–145. https://doi.org/10.1242/jeb.124941

Gautel, M., D. Goulding, B. Bullard, K. Weber, and D.O. Fürst. 1996. The central Z-disk region of titin is assembled from a novel repeat in variable copy numbers. *J. Cell Sci.* 109:2747–2754.

Gombos, R., E. Migh, O. Antal, A. Mukherjee, A. Jenny, and J. Mihaly. 2015. The Formin DAAM Functions as Molecular Effector of the Planar Cell Polarity Pathway during Axonal Development in Drosophila. *J. Neurosci.* 35:10154–10167. https://doi.org/10.1523/JNEUROSCI.3708-14.2015

Gonzalez-Morales, N., T.K. Holenka, and F. Schock. 2017. Filamin actin-binding and titin-binding fulfill distinct functions in Z-disc cohesion. *PLoS Genet.* 13:e1006880. https://doi.org/10.1371/journal.pgen.1006880

Greenfield, N.J., A.S. Kostyukova, and S.E. Hitchcock-DeGregori. 2005. Structure and tropomyosin binding properties of the N-terminal capping domain of tropomodulin 1. *Biophys. J.* 88:372–383. https://doi.org/10.1529/biophysj.104.051128

Hakeda, S., S. Endo, and K. Saigo. 2000. Requirements of Kettin, a giant muscle protein highly conserved in overall structure in evolution, for normal muscle function, viability, and flight activity of Drosophila. *J. Cell Biol.* 148:101–114. https://doi.org/10.1083/jcb.148.1.101

Hanke, P.D., and R.V. Storti. 1988. The Drosophila melanogaster tropomyosin II gene produces multiple proteins by use of alternative tissue-specific promoters and alternative splicing. *Mol. Cell. Biol.* 8:3591–3602. https://doi.org/10.1128/MCB.8.9.3591

Heilemann, M., S. van de Linde, M. Schüttpelz, R. Kasper, B. Seefeldt, A. Mukherjee, P. Tinnefeld, and M. Sauer. 2008. Subdiffraction-resolution fluorescence imaging with conventional fluorescent probes. *Angew. Chem. Int. Ed. Engl.* 47:6172–6176. https://doi.org/10.1002/anie.200802376

Hess, S.T., T.P. Girirajan, and M.D. Mason. 2006. Ultra-high resolution imaging by fluorescence photoactivation localization microscopy. *Biophys. J.* 91:4258–4272. https://doi.org/10.1529/biophysj.106.091116

Higashi, T., T. Ikeda, T. Murakami, R. Shirakawa, M. Kawato, K. Okawa, M. Furuse, T. Kimura, T. Kita, and H. Horiuchi. 2010. Flightless-I (Fli-I) regulates the actin assembly activity of diaphanous-related formins (DRFs) Daam1 and mDia1 in cooperation with active Rho GTPase. *J. Biol. Chem.* 285:16231–16238. https://doi.org/10.1074/jbc.M109.079236

Hiromi, Y., and Y. Hotta. 1985. Actin gene mutations in Drosophila; heat shock activation in the indirect flight muscles. *EMBO J.* 4:1681–1687. https://doi.org/10.1002/j.1460-2075.1985.tb03837.x

Hu, Z., D.W. Taylor, M.K. Reedy, R.J. Edwards, and K.A. Taylor. 2016. Structure of myosin filaments from relaxed *Lethocerus* flight muscle by cryo-EM at 6 Å resolution. *Sci. Adv.* 2:e1600058. https://doi.org/10.1126/sciadv.1600058

Hu, Z., D.W. Taylor, R.J. Edwards, and K.A. Taylor. 2017. Coupling between myosin head conformation and the thick filament backbone structure. *J. Struct. Biol.* 200:334–342. https://doi.org/10.1016/j.jsb.2017.09.009

Huang, B., M. Bates, and X. Zhuang. 2009. Super-resolution fluorescence microscopy. *Annu. Rev. Biochem.* 78:993–1016. https://doi.org/10.1146/annurev.biochem.77.061906.092014

Iwamoto, H. 2013. The long C-terminal extension of insect flight muscle-specific troponin-I isoform is not required for stretch activation. *Biochem. Biophys. Res. Commun.* 431:47–51. https://doi.org/10.1016/j.bbrc.2012.12.101

Källberg, M., H. Wang, S. Wang, J. Peng, Z. Wang, H. Lu, and J. Xu. 2012. Template-based protein structure modeling using the RaptorX web server. *Nat. Protoc.* 7:1511–1522. https://doi.org/10.1038/nprot.2012.085

Karlik, C.C., and E.A. Fyrberg. 1986. Two Drosophila melanogaster tropomyosin genes: structural and functional aspects. *Mol. Cell. Biol.* 6: 1965–1973. https://doi.org/10.1128/MCB.6.6.1965

Katzemich, A., J.Y. Long, K. Jani, B.R. Lee, and F. Schöck. 2011. Muscle type-specific expression of Zasp52 isoforms in Drosophila. *Gene Expr. Patterns.* 11:484–490. https://doi.org/10.1016/j.gep.2011.08.004

Katzemich, A., N. Kreisköther, A. Alexandrovich, C. Elliott, F. Schöck, K. Leonard, J. Sparrow, and B. Bullard. 2012. The function of the M-line protein obscurin in controlling the symmetry of the sarcomere in the flight muscle of Drosophila. *J. Cell Sci.* 125:3367–3379. https://doi.org/10.1242/jcs.097345

Katzemich, A., K.A. Liao, S. Czerniecki, and F. Schöck. 2013. Alp/Enigma family proteins cooperate in Z-disc formation and myofibril assembly. *PLoS Genet.* 9:e1003342. https://doi.org/10.1371/journal.pgen.1003342

Katzemich, A., R.J. West, A. Fukuzawa, S.T. Sweeney, M. Gautel, J. Sparrow, and B. Bullard. 2015. Binding partners of the kinase domains in Drosophila obscurin and their effect on the structure of the flight muscle. *J. Cell Sci.* 128:3386–3397. https://doi.org/10.1242/jcs.170639

Klein, T., S. Proppert, and M. Sauer. 2014. Eight years of single-molecule localization microscopy. *Histochem. Cell Biol.* 141:561–575. https://doi.org/10.1007/s00418-014-1184-3

Koana, T., and Y. Hotta. 1978. Isolation and characterization of flightless mutants in Drosophila melanogaster. *J. Embryol. Exp. Morphol.* 45: 123–143.

Kooij, V., M.C. Viswanathan, D.I. Lee, P.P. Rainer, W. Schmidt, W.A. Kronert, S.E. Harding, D.A. Kass, S.I. Bernstein, J.E. Van Eyk, and A. Cammarato. 2016. Profilin modulates sarcomeric organization and mediates cardiomyocyte hypertrophy. *Cardiovasc. Res.* 110:238–248. https://doi.org/10.1093/cvr/cvw050

Kulke, M., C. Neagoe, B. Kolmerer, A. Minajeva, H. Hinssen, B. Bullard, and W.A. Linke. 2001. Kettin, a major source of myofibrillar stiffness in Drosophila indirect flight muscle. *J. Cell Biol.* 154:1045–1058. https://doi.org/10.1083/jcb.200104016

Külshammer, E., and M. Uhlirova. 2013. The actin cross-linker Filamin/Cheerio mediates tumor malignancy downstream of JNK signaling. *J. Cell Sci.* 126:927–938. https://doi.org/10.1242/jcs.114462

Lakey, A., C. Ferguson, S. Labeit, M. Reedy, A. Larkins, G. Butcher, K. Leonard, and B. Bullard. 1990. Identification and localization of high molecular weight proteins in insect flight and leg muscle. *EMBO J.* 9: 3459–3467. https://doi.org/10.1002/j.1460-2075.1990.tb07554.x

Li, M.G., M. Serr, K. Edwards, S. Ludmann, D. Yamamoto, L.G. Tilney, C.M. Field, and T.S. Hays. 1999. Filamin is required for ring canal assembly and actin organization during Drosophila oogenesis. *J. Cell Biol.* 146: 1061–1074. https://doi.org/10.1083/jcb.146.5.1061

Liao, K.A., N. Gonzalez-Morales, and F. Schock. 2016. Zasp52, a Core Z-disc Protein in Drosophila Indirect Flight Muscles, Interacts with alpha-Actinin via an Extended PDZ Domain. *PLoS Genet.* 12:e1006400. https://doi.org/10.1371/journal.pgen.1006400

Littlefield, R., A. Almenar-Queralt, and V.M. Fowler. 2001. Actin dynamics at pointed ends regulates thin filament length in striated muscle. *Nat. Cell Biol.* 3:544–551. https://doi.org/10.1038/35078517

Liu, J., D.W. Taylor, E.B. Krementsova, K.M. Trybus, and K.A. Taylor. 2006. Three-dimensional structure of the myosin V inhibited state by cryoelectron tomography. *Nature.* 442:208–211. https://doi.org/10.1038/nature04719

Luther, P.K. 2009. The vertebrate muscle Z-disc: sarcomere anchor for structure and signalling. *J. Muscle Res. Cell Motil.* 30:171–185. https://doi.org/10.1007/s10974-009-9189-6

Luther, P.K., R. Padrón, S. Ritter, R. Craig, and J.M. Squire. 2003. Heterogeneity of Z-band structure within a single muscle sarcomere: implications for sarcomere assembly. *J. Mol. Biol.* 332:161–169. https://doi.org/10.1016/S0022-2836(03)00883-0

Machado, C., and D.J. Andrew. 2000. D-Titin: a giant protein with dual roles in chromosomes and muscles. *J. Cell Biol.* 151:639–652. https://doi.org/10.1083/jcb.151.3.639

Mannherz, H.G., R.S. Goody, M. Konrad, and E. Nowak. 1980. The interaction of bovine pancreatic deoxyribonuclease I and skeletal muscle actin. *Eur. J. Biochem.* 104:367–379. https://doi.org/10.1111/j.1432-1033.1980.tb04437.x

Mardahl-Dumesnil, M., and V.M. Fowler. 2001. Thin filaments elongate from their pointed ends during myofibril assembly in Drosophila indirect flight muscle. *J. Cell Biol.* 155:1043–1053. https://doi.org/10.1083/jcb.200108026

Mateos, J., R. Herranz, A. Domingo, J. Sparrow, and R. Marco. 2006. The structural role of high molecular weight tropomyosins in dipteran indirect flight muscle and the effect of phosphorylation. *J. Muscle Res. Cell Motil.* 27:189–201. https://doi.org/10.1007/s10974-005-9044-3

Matusek, T., A. Djiane, F. Jankovics, D. Brunner, M. Mlodzik, and J. Mihály. 2006. The Drosophila formin DAAM regulates the tracheal cuticle pattern through organizing the actin cytoskeleton. *Development.* 133:957–966. https://doi.org/10.1242/dev.02266

Miklos, G.L., and H.G. De Couet. 1990. The mutations previously designated as flightless-I3, flightless-O2 and standby are members of the W-2 lethal complementation group at the base of the X-chromosome of Drosophila melanogaster. *J. Neurogenet.* 6:133–151. https://doi.org/10.3109/01677069009107106

Miller, A., and R.T. Tregear. 1972. Structure of insect fibrillar flight muscle in the presence and absence of ATP. *J. Mol. Biol.* 70:85–104. https://doi.org/10.1016/0022-2836(72)90165-9

Molnár, I., E. Migh, S. Szikora, T. Kalmár, A.G. Végh, F. Deák, S. Barkó, B. Bugyi, Z. Orfanos, J. Kovács, et al. 2014. DAAM is required for thin filament formation and Sarcomerogenesis during muscle development in Drosophila. *PLoS Genet.* 10:e1004166. https://doi.org/10.1371/journal.pgen.1004166

Orfanos, Z., and J.C. Sparrow. 2013. Myosin isoform switching during assembly of the Drosophila flight muscle thick filament lattice. *J. Cell Sci.* 126:139–148. https://doi.org/10.1242/jcs.110361

Pettersen, E.F., T.D. Goddard, C.C. Huang, G.S. Couch, D.M. Greenblatt, E.C. Meng, and T.E. Ferrin. 2004. UCSF Chimera--a visualization system for exploratory research and analysis. *J. Comput. Chem.* 25:1605–1612. https://doi.org/10.1002/jcc.20084

Qiu, F., A. Lakey, B. Agianian, A. Hutchings, G.W. Butcher, S. Labeit, K. Leonard, and B. Bullard. 2003. Troponin C in different insect muscle types: identification of two isoforms in Lethocerus, Drosophila and Anopheles that are specific to asynchronous flight muscle in the adult insect. *Biochem. J.* 371:811–821. https://doi.org/10.1042/bj20021814

Rao, J.N., Y. Madasu, and R. Dominguez. 2014. Mechanism of actin filament pointed-end capping by tropomodulin. *Science.* 345:463–467. https://doi.org/10.1126/science.1256159

Reedy, M.C., and C. Beall. 1993. Ultrastructure of developing flight muscle in Drosophila. I. Assembly of myofibrils. *Dev. Biol.* 160:443–465. https://doi.org/10.1006/dbio.1993.1320

Reedy, M.C., and B. Bullard. 1996. The Insect Flight Muscle Sarcomere as a Model System for Immunolocalization. *Methods.* 10:219–233. https://doi.org/10.1006/meth.1996.0097

Reedy, M.K., and M.C. Reedy. 1985. Rigor crossbridge structure in tilted single filament layers and flared-X formations from insect flight muscle. *J. Mol. Biol.* 185:145–176. https://doi.org/10.1016/0022-2836(85)90188-3

Rees, E.J., M. Erdelyi, G.S.K. Schierle, A. Knight, and C.F. Kaminski. 2013. Elements of image processing in localization microscopy. *J. Opt.* 15:094012. https://doi.org/10.1088/2040-8978/15/9/094012

RStudio Team. 2015. RStudio: Integrated Development for R. RStudio, Inc., Boston, MA. Available at: http://www.rstudio.com (accessed on July 16, 2018).

Rust, M.J., M. Bates, and X. Zhuang. 2006. Sub-diffraction-limit imaging by stochastic optical reconstruction microscopy (STORM). *Nat. Methods.* 3:793–795. https://doi.org/10.1038/nmeth929

Rusu, M., Z. Hu, K.A. Taylor, and J. Trinick. 2017. Structure of isolated Z-disks from honeybee flight muscle. *J. Muscle Res. Cell Motil.* 38:241–250. https://doi.org/10.1007/s10974-017-9477-5

Saide, J.D., S. Chin-Bow, J. Hogan-Sheldon, L. Busquets-Turner, J.O. Vigoreaux, K. Valgeirsdottir, and M.L. Pardue. 1989. Characterization of components of Z-bands in the fibrillar flight muscle of Drosophila melanogaster. *J. Cell Biol.* 109:2157–2167. https://doi.org/10.1083/jcb.109.5.2157

Schmitz, H., C. Lucaveche, M.K. Reedy, and K.A. Taylor. 1994. Oblique section 3-D reconstruction of relaxed insect flight muscle reveals the cross-bridge lattice in helical registration. *Biophys. J.* 67:1620–1633. https://doi.org/10.1016/S0006-3495(94)80635-6

Schnorrer, F., C. Schönbauer, C.C. Langer, G. Dietzl, M. Novatchkova, K. Schernhuber, M. Fellner, A. Azaryan, M. Radolf, A. Stark, et al. 2010. Systematic genetic analysis of muscle morphogenesis and function in Drosophila. *Nature.* 464:287–291. https://doi.org/10.1038/nature08799

Shwartz, A., N. Dhanyasi, E.D. Schejter, and B.Z. Shilo. 2016. The Drosophila formin Fhos is a primary mediator of sarcomeric thin-filament array assembly. *eLife.* 5:e16540. https://doi.org/10.7554/eLife.16540

Sigal, Y.M., R.B. Zhou, and X.W. Zhuang. 2018. Visualizing and discovering cellular structures with super-resolution microscopy. *Science.* 361:880–887. https://doi.org/10.1126/science.aau1044

Spletter, M.L., C. Barz, A. Yeroslaviz, X. Zhang, S.B. Lemke, A. Bonnard, E. Brunner, G. Cardone, K. Basler, B.H. Habermann, and F. Schnorrer. 2018. A transcriptomics resource reveals a transcriptional transition during ordered sarcomere morphogenesis in flight muscle. *eLife.* 7:e34058. https://doi.org/10.7554/eLife.34058

Squire, J.M., H.A. Al-Khayat, C. Knupp, and P.K. Luther. 2005. Molecular architecture in muscle contractile assemblies. *Adv. Protein Chem.* 71:17–87. https://doi.org/10.1016/S0065-3233(04)71002-5

Squire, J.M., T. Bekyarova, G. Farman, D. Gore, G. Rajkumar, C. Knupp, C. Lucaveche, M.C. Reedy, M.K. Reedy, and T.C. Irving. 2006. The myosin filament superlattice in the flight muscles of flies: A-band lattice optimisation for stretch-activation? *J. Mol. Biol.* 361:823–838. https://doi.org/10.1016/j.jmb.2006.06.072

Sulbaran, G., L. Alamo, A. Pinto, G. Marquez, F. Mendez, R. Padron, and R. Craig. 2015. An invertebrate smooth muscle with striated muscle myosin filaments. *Proc. Natl. Acad. Sci. USA.* 112:E5660–E5668. https://doi.org/10.1073/pnas.1513439112

Trombitás, K., and H. Granzier. 1997. Actin removal from cardiac myocytes shows that near Z line titin attaches to actin while under tension. *Am. J. Physiol.* 273:C662–C670. https://doi.org/10.1152/ajpcell.1997.273.2.C662

van de Linde, S., A. Löschberger, T. Klein, M. Heidbreder, S. Wolter, M. Heilemann, and M. Sauer. 2011. Direct stochastic optical reconstruction microscopy with standard fluorescent probes. *Nat. Protoc.* 6:991–1009. https://doi.org/10.1038/nprot.2011.336

van Straaten, M., D. Goulding, B. Kolmerer, S. Labeit, J. Clayton, K. Leonard, and B. Bullard. 1999. Association of kettin with actin in the Z-disc of insect flight muscle. *J. Mol. Biol.* 285:1549–1562. https://doi.org/10.1006/jmbi.1998.2386

Verheyen, E.M., and L. Cooley. 1994. Profilin mutations disrupt multiple actin-dependent processes during Drosophila development. *Development.* 120:717–728.

Vigoreaux, J. 2007. Nature's Versatile Engine: Insect Flight Muscle Inside and Out. Springer Science & Business Media, New York.

von der Ecken, J., M. Müller, W. Lehman, D.J. Manstein, P.A. Penczek, and S. Raunser. 2015. Structure of the F-actin-tropomyosin complex. *Nature.* 519:114–117. https://doi.org/10.1038/nature14033

Wendt, T., and K. Leonard. 1999. Structure of the insect troponin complex. *J. Mol. Biol.* 285:1845–1856. https://doi.org/10.1006/jmbi.1998.2414

Wendt, T., V. Guénebaut, and K.R. Leonard. 1997. Structure of the Lethocerus troponin-tropomyosin complex as determined by electron microscopy. *J. Struct. Biol.* 118:1–8. https://doi.org/10.1006/jsbi.1996.3834

Wu, S., J. Liu, M.C. Reedy, R.T. Tregear, H. Winkler, C. Franzini-Armstrong, H. Sasaki, C. Lucaveche, Y.E. Goldman, M.K. Reedy, and K.A. Taylor. 2010. Electron tomography of cryofixed, isometrically contracting insect flight muscle reveals novel actin-myosin interactions. *PLoS One.* 5:e12643. https://doi.org/10.1371/journal.pone.0012643

Young, P., E. Ehler, and M. Gautel. 2001. Obscurin, a giant sarcomeric Rho guanine nucleotide exchange factor protein involved in sarcomere assembly. *J. Cell Biol.* 154:123–136. https://doi.org/10.1083/jcb.200102110

JCB

Supplemental material

Szikora et al., https://doi.org/10.1083/jcb.201907026

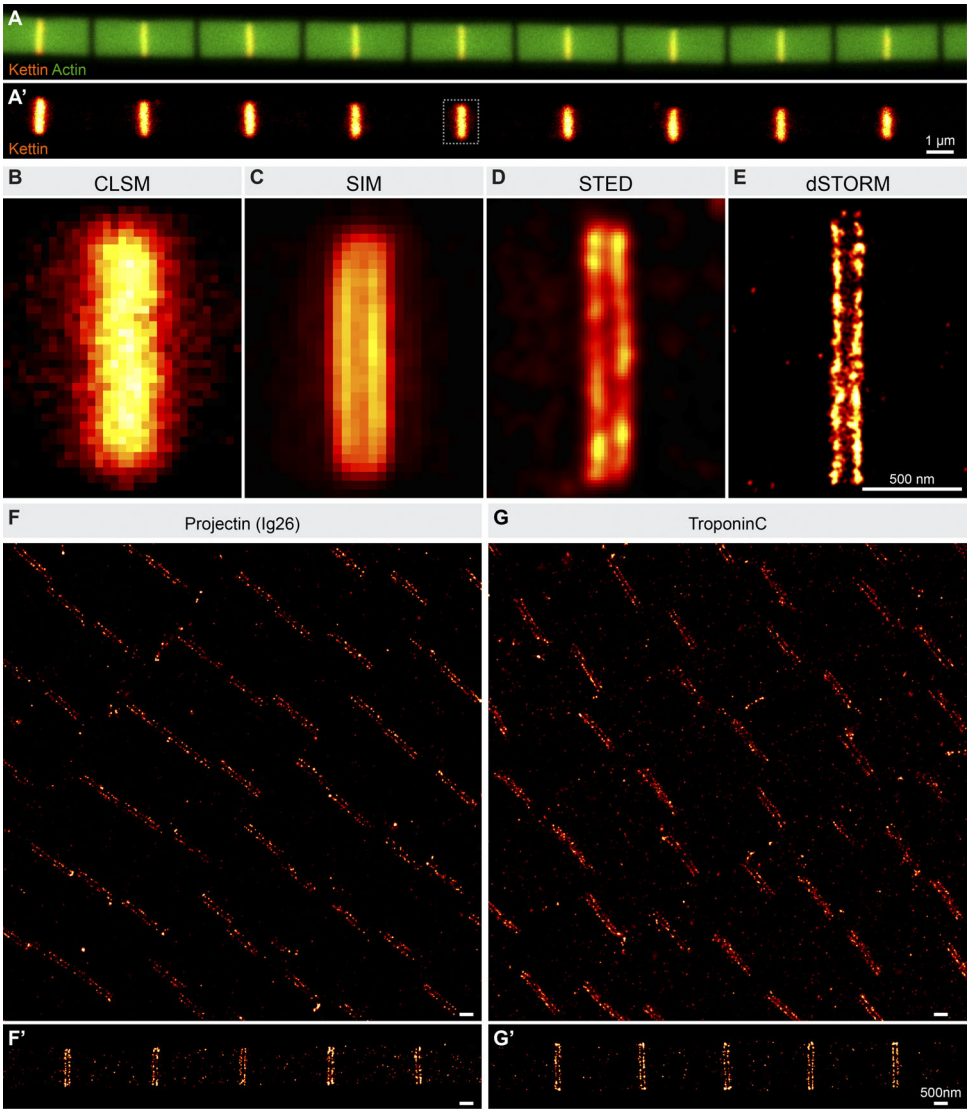

Figure S1. **Individual myofibrils of the *Drosophila* IFMs are ideal for dSTORM imaging. (A and A′)** Confocal imaging of the individual myofibrils nicely reveals actin organization and Kettin accumulation at the Z-disk. Scale bar, 1 µm. **(B–E)** The Kettin signal at the Z-disk appears as a single band with CLSM (B) that can be resolved into two individual bands with superresolution approaches such as SIM (C), STED (D), and dSTORM (E), of which dSTORM clearly provides the highest resolution. Scale bar, 500 nm. **(F–G′)** Comparison of the nanoscopic localization of Projectin (Ig26) and TnC in dissected intact flight muscles (F and G) with that in individual myofibrils (F′ and G′) reveals a highly similar pattern. Scale bars, 500 nm.

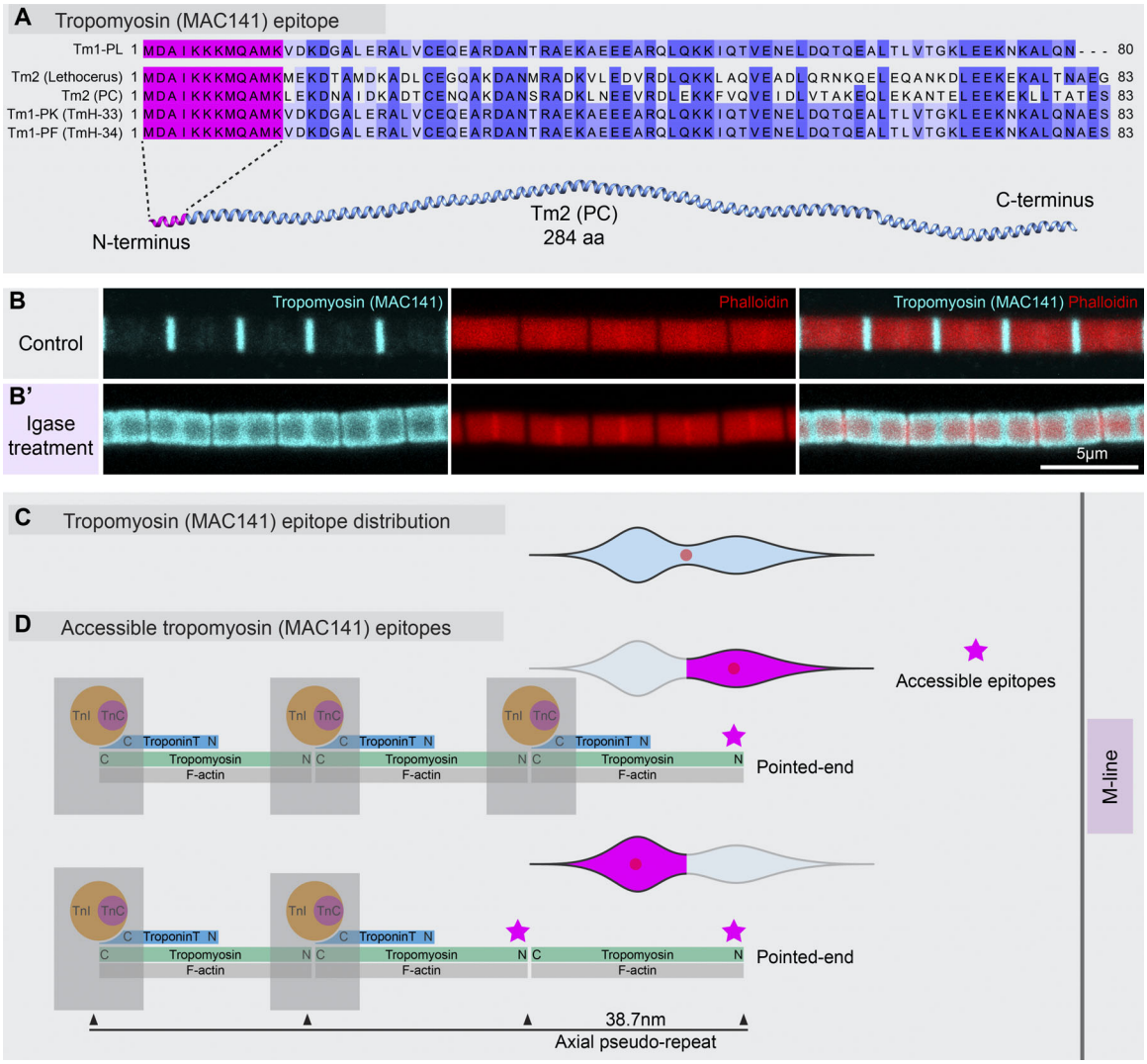

Figure S2. **Tm (MAC141) epitope position and distribution. (A)** The epitope recognized by the monoclonal MAC141 antibody has been restricted to an 80-aa-long N-terminal sequence in Tm1-PL, and this antibody is known to recognize all IFM-specific Tm isoforms (Tm2, TmH-33, and TmH-34). Sequence comparison suggests that the MAC141 epitope is most likely within a 12-aa-long conserved N-terminal region (highlighted in magenta). **(B)** MAC141 staining of wild-type IFM myofibrils displays a strong signal in the H-zone and a faint signal in the A-band. Nanoscopy revealed that the H-zone accumulation corresponds to a double line structure close to the pointed ends. This suggests that the epitope recognized by MAC141 is close to the pointed ends but largely masked along the rest of the thin filaments. **(B′)** Myofibrils treated with the Igase enzyme to remove the hydrophobic extensions of TmH-34, thereby loosening up the Tn bridges, exhibit a nearly uniform MAC141 staining along the A-bands. This observation supports the idea that the epitope is masked in the A-band and it is located on the N-terminus. Scale bar, 5 µm. **(C and D)** Unlike in the I-band where Tm exhibit a double-line-type distribution with one single peak on both sides of the Z-line, the MAC141 signal in the H-zone appears as a double peak on either side of the M-line (schematized in C). The M-ward peak of the doublet corresponds exactly to the pointed-end region, whereas the other marks the middle of the most proximal axial repeat (D). The I-band distribution and position of the M-ward H-zone peak is entirely consistent with an N-terminal epitope localization. With regard to the peak in the middle of the most proximal axial repeat, we propose that it could be the average position of the two most M-ward epitopes by assuming that the most proximal Tn complex is missing from some of the thin filaments, which makes those epitopes accessible (stars).

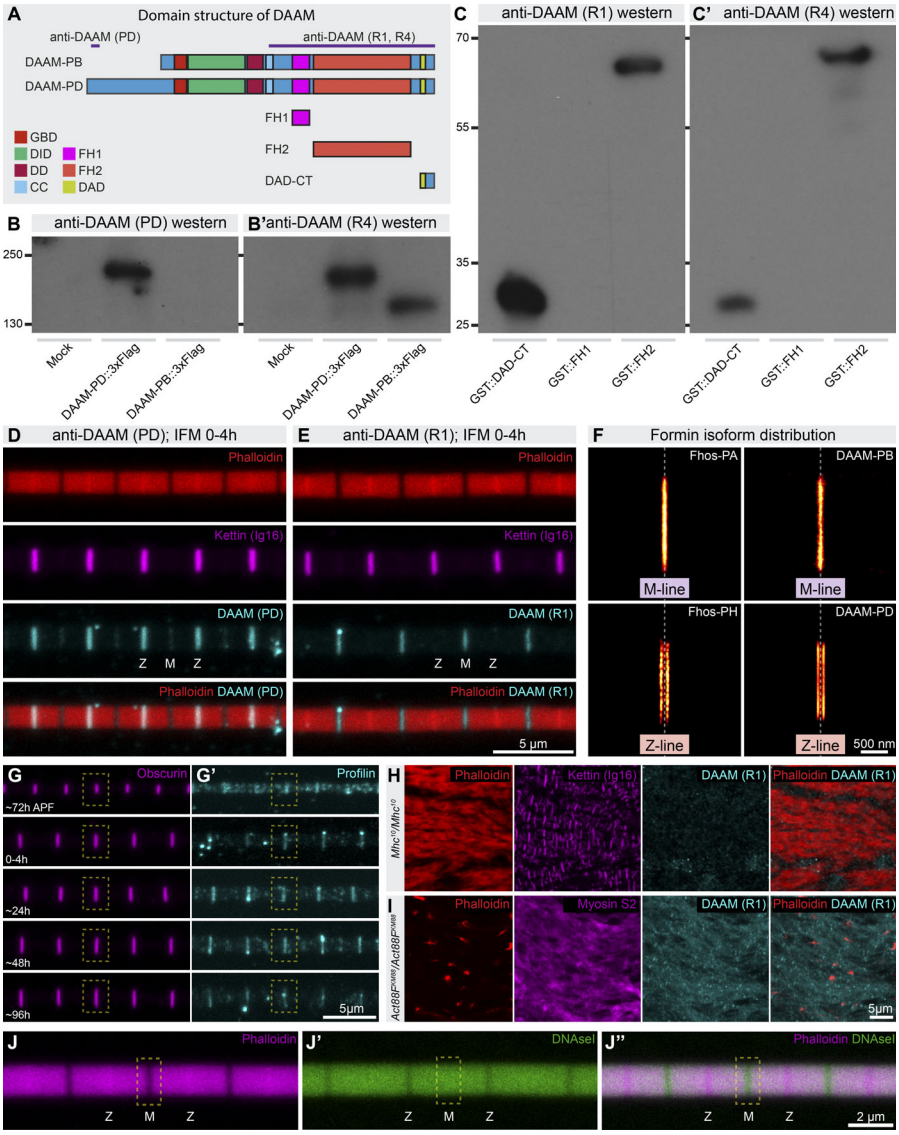

Figure S3. **The short and long isoforms of DAAM and the localization of Profilin. (A)** Domain structure of the two DAAM isoforms, PB and PD, expressed in the IFM. Note that the two isoforms are completely overlapping, while the PD isoform contains an N-terminal extension of 310 aa. The anti-DAAM (PD) serum was raised against an N-terminal, PD isoform–specific peptide, whereas the (R1) antibody was raised against a C-terminal region of the protein, present in both isoforms. **(B and B′)** Western blots show that, as expected, the (R4) antibody (raised against the same sequences as R1) recognizes the short (PB) and long (PD) isoform, while the anti-DAAM (PD) recognizes only the long isoform from S2 cell lysates transfected with DAAM-PB– or DAAM-PD–expressing constructs. **(C and C′)** Western blots with bacterially expressed proteins reveal that R1 and R4 both recognize the FH2 and DAD-CT regions but not the FH1 domain. It is of note that R1 appears to exhibit a much higher affinity for DAD-CT than R4. **(D and E)** Anti-DAAM (PD) staining in a 0–4 h IFM reveals a strong accumulation at the Z-disk and a weak signal at the M-line; conversely, (R1) displays a strong signal at the M-line and a very weak if any enrichment at the Z-disk. Thus, it appears that although (R1) recognizes both isoforms in denaturing conditions (i.e., after SDS-PAGE), when used for immunohistochemistry, it is specific for the short isoform. In addition, these results indicate that in these young IFMs, the PD isoform is enriched at the Z-disk, whereas the PB isoform accumulates at the M-line. Scale bar, 5 µm. **(F)** Comparison of the nanoscopic distribution of the two Fhos and two DAAM isoforms in the IFM demonstrates that the short isoforms (Fhos-PA and DAAM-PB) are enriched in a narrow stripe at the M-line, while the long isoforms (Fhos-PH and DAAM-PD) accumulate in two stripes along the Z-line. This differential distribution is likely to indicate an isoform specific in vivo function at the Z-disk versus the M-line, for example the short isoforms promote pointed end elongation while the long isoforms are involved in barbed end dynamics. Scale bar, 500 nm. **(G and G′)** Developmental analysis of Profilin accumulation in the IFM. Whereas former work suggested that Profilin accumulates at the Z-disk, we found that, in addition to a weak staining along the entire myofibril, the bulk of the protein is enriched at the M-line (indicated by the colocalization with Obscurin) in the IFM of 24-h-old adults. To rule out the possibility that Profilin expression displays a different pattern during development, we examined its distribution in two earlier (72 h after puparium formation [APF] and 0–4 h adult) and two later (48 h and 96 h adult) developmental time points. This analysis confirmed the M-line association at each developmental stage, although the enrichment looked somewhat less specific in 72-h-APF myofibrils. Scale bar, 5 µm. **(H and I)** Sarcomere association of DAAM depends on Mhc. **(H)** Confocal images show that DAAM localization in an *Mhc*-null mutant myofibril is virtually lost. **(I)** In *Act88F*-null mutant IFMs, a residual DAAM accumulation is clearly visible. In agreement with its nanoscopic protein distribution at the M-line, these data suggest that myofibril association of at least the short isoform of DAAM, recognized by R1 in 0–4 h IFM, primarily depends on Mhc and not on actin. **(J–J″)** Myofibrillar G-actin distribution was visualized with deoxyribonuclease I (DNaseI) staining, which revealed a nearly uniform localization along the entire myofibril but at the Z-disk, where the staining is much weaker than elsewhere. This result clearly confirms the presence of G-actin in the H-zone. Scale bar, 5 µm.

Table S1. **List of primary antibodies used in this study**

Protein target	Name	Antigen	Host species	Dilution	Source/supplier	Reference
Actin	Actin (rat)	Monoclonal antibody reacts with actin and arthrin	Rat	1:200	Babraham MAC 237	Lakey et al., 1990
Actin	Actin (C4)	Epitope appears to be located in the N-terminus, possibly near amino acids 50–70	Mouse	1:200	Cedarlane Laboratories	
Cpa	Cpa	Antibody was raised against full-length Cpa sequence	Rabbit	1:100	Florence Janody	Amândio et al., 2014
DAAM	DAAM (R1)	Antibody was raised to the C-terminal half (C-DAAM) of the protein; "R1"	Rabbit	1:1,000	Our laboratory	Matusek et al., 2006
DAAM	DAAM (PD)	Antibody was raised against an N-terminal polypeptide corresponding to amino acid residues 26–43 of the DAAM-PD; "PD756 INEP"	Rabbit	1:1,000	Our laboratory	This study
Fhos	Fhos	Antibody was raised to the 93 C-terminal residues of the Fhos protein	Rat	1:100	Ben-Zion Shilo	Shwartz et al., 2016
FLN	FLN (C-term)	Epitope is located in the last 90 C-terminal residues; "43-D"	Rabbit	1:100	Thomas Hays	Li et al., 1999
FLN	FLN (N-term)	Epitope is located in the N-terminus (residues 189–482)	Rat	1:100	Mirka Uhlirova	Külshammer and Uhlirova, 2013
FliI	FliI	Antibody was raised to the N-terminus of FliI (human origin; "(116.40): sc-21716"	Mouse	1:50	Santa Cruz Biotechnology	
Kettin	Kettin (Ig34)	Epitope is located in the Ig34–Ig35 region; "K40"	Rabbit	1:200	Belinda Bullard	Kulke et al., 2001
Kettin, Sls700	Kettin (Ig16)	Epitope is located in the linker-Ig16-linker region	Rat	1:200	Babraham MAC 155	Lakey et al., 1990
Mhc	Myosin S2	Monoclonal antibody reacts with subfragment 2 of Mhc	Rat	1:200	Babraham MAC 147	Fyrberg et al., 1990
Obscurin	Obscurin (Ig14-16)	Epitope is located in the Ig14-Ig15-Ig16 region	Rabbit	1:400	Belinda Bullard	Burkart et al., 2007
Obscurin	Obscurin (Kin1)	Rabbit antibody was raised against kinase1 domain.	Rabbit	1:400	Belinda Bullard	Katzemich et al., 2012
Profilin	Profilin	Antibody was raised against the full-length chickadee sequence; "chi 1J"	Mouse	1:10	DSHB	Verheyen and Cooley, 1994
Projectin	Projectin (Ig26)	Epitope is located in the Ig26 domain	Rat	1:200	Babraham MAC 150	Lakey et al., 1990
Projectin	Projectin (P5)	Not known	Mouse	1:300	DSHB	Saide et al., 1989
SALS	SALS	Antibody was raised to the 388–594 region; "anti-SALS-Bai"	Rabbit	1:400	Norbert Perrimon	Bai et al., 2007
Sls700	Sls700 (B2)	Epitope is located within a three Ig domain containing region from exon 22	Rabbit	1:200	Belinda Bullard	Burkart et al., 2007
Tmod	Tmod	Not known	Rat	1:200	Velia Fowler	
Tm	Tm	Antibody reacts with Tm (TmH-33 and TmH-34)	Rat	1:400	Babraham MAC 141	Bullard et al., 1988
TmH-34	TmH-34	Antibody reacts with the 34 isoform of TmH Antibody also reacts with GST-2 kin and BiP (hsc72)	Rat	1:200	Babraham MAC 143	Bullard et al., 1988
Tn C	Tn C	Antibody reacts with TnC isoforms F1 and F2 in flight muscle and with Tn C in nonflight muscles	Rat	1:200	Babraham MAC 352	Qiu et al., 2003
Tn T	Tn T	Antibody reacts with TnT in *Lethocerus*, *Drosophila*, and dragonfly muscles (flight and nonflight)	Rat	1:200	Babraham MAC 145	Bullard et al., 1988
Zasp52	Zasp52	Epitope is located in the sequence encoded by exon 16; "1D3-3E4"	Mouse	1:400	DSHB	Saide et al., 1989
Zormin	Zormin (B1)	Epitope is located in the Ig4-Ig5-Ig6 region; "B1"	Rabbit	1:200	Belinda Bullard	Burkart et al., 2007
α-Actinin	α-Actinin	Monoclonal antibody reacts with α-Actinin	Rat	1:200	Babraham MAC 276	Lakey et al., 1990

Provided online is a supplemental figure PDF showing an overview of the imaged sarcomeric proteins. A representative CLSM image, a collection of representative individual dSTORM images, and an aligned and averaged dSTORM image is presented for every antibody. Scale bar, 500 nm. Measured epitope distributions relative to the Z- or M-line, depicted as violin plots (mean ± SD), are shown on the right. Mean values are indicated with red dots. Schematic diagrams of the depicted proteins are drawn to scale (on the left). The important domains are represented on enlarged diagrams where appropriate. Known epitope positions are also indicated in purple and cyan lines (see also Table S1). The corresponding protein structures are generally presented as in the models (using the same color code), with the exception of the large modular proteins, which are straightened to demonstrate their length. Arrows on the rightmost (upper and lower) individual dSTORM images of Zasp52 indicate regions where a double-line-type distribution can be appreciated. More detailed explanations are provided for each molecule and measurement in the main text and the model constructing part of Materials and methods. Scale bar, 10 nm.

References

Amândio, A.R., P. Gaspar, J.L. Whited, and F. Janody. 2014. Subunits of the Drosophila actin-capping protein heterodimer regulate each other at multiple levels. *PLoS One.* 9:e96326. https://doi.org/10.1371/journal.pone.0096326

Bai, J., J.H. Hartwig, and N. Perrimon. 2007. SALS, a WH2-domain-containing protein, promotes sarcomeric actin filament elongation from pointed ends during Drosophila muscle growth. *Dev. Cell.* 13:828–842. https://doi.org/10.1016/j.devcel.2007.10.003

Bullard, B., K. Leonard, A. Larkins, G. Butcher, C. Karlik, and E. Fyrberg. 1988. Troponin of asynchronous flight muscle. *J. Mol. Biol.* 204:621–637. https://doi.org/10.1016/0022-2836(88)90360-9

Burkart, C., F. Qiu, S. Brendel, V. Benes, P. Hååg, S. Labeit, K. Leonard, and B. Bullard. 2007. Modular proteins from the Drosophila sallimus (sls) gene and their expression in muscles with different extensibility. *J. Mol. Biol.* 367:953–969. https://doi.org/10.1016/j.jmb.2007.01.059

Fyrberg, E., C.C. Fyrberg, C. Beall, and D.L. Saville. 1990. Drosophila melanogaster troponin-T mutations engender three distinct syndromes of myofibrillar abnormalities. *J. Mol. Biol.* 216:657–675. https://doi.org/10.1016/0022-2836(90)90390-8

Katzemich, A., N. Kreisköther, A. Alexandrovich, C. Elliott, F. Schöck, K. Leonard, J. Sparrow, and B. Bullard. 2012. The function of the M-line protein obscurin in controlling the symmetry of the sarcomere in the flight muscle of Drosophila. *J. Cell Sci.* 125:3367–3379. https://doi.org/10.1242/jcs.097345

Kulke, M., C. Neagoe, B. Kolmerer, A. Minajeva, H. Hinssen, B. Bullard, and W.A. Linke. 2001. Kettin, a major source of myofibrillar stiffness in Drosophila indirect flight muscle. *J. Cell Biol.* 154:1045–1057. https://doi.org/10.1083/jcb.200104016

Külshammer, E., and M. Uhlirova. 2013. The actin cross-linker Filamin/Cheerio mediates tumor malignancy downstream of JNK signaling. *J. Cell Sci.* 126: 927–938. https://doi.org/10.1242/jcs.114462

Lakey, A., C. Ferguson, S. Labeit, M. Reedy, A. Larkins, G. Butcher, K. Leonard, and B. Bullard. 1990. Identification and localization of high molecular weight proteins in insect flight and leg muscle. *EMBO J.* 9:3459–3467. https://doi.org/10.1002/j.1460-2075.1990.tb07554.x

Li, M.G., M. Serr, K. Edwards, S. Ludmann, D. Yamamoto, L.G. Tilney, C.M. Field, and T.S. Hays. 1999. Filamin is required for ring canal assembly and actin organization during Drosophila oogenesis. *J. Cell Biol.* 146:1061–1074. https://doi.org/10.1083/jcb.146.5.1061

Matusek, T., A. Djiane, F. Jankovics, D. Brunner, M. Mlodzik, and J. Mihály. 2006. The Drosophila formin DAAM regulates the tracheal cuticle pattern through organizing the actin cytoskeleton. *Development.* 133:957–966. https://doi.org/10.1242/dev.02266

Qiu, F., A. Lakey, B. Agianian, A. Hutchings, G.W. Butcher, S. Labeit, K. Leonard, and B. Bullard. 2003. Troponin C in different insect muscle types: identification of two isoforms in Lethocerus, Drosophila and Anopheles that are specific to asynchronous flight muscle in the adult insect. *Biochem. J.* 371: 811–821. https://doi.org/10.1042/bj20021814

Saide, J.D., S. Chin-Bow, J. Hogan-Sheldon, L. Busquets-Turner, J.O. Vigoreaux, K. Valgeirsdottir, and M.L. Pardue. 1989. Characterization of components of Z-bands in the fibrillar flight muscle of Drosophila melanogaster. *J. Cell Biol.* 109:2157–2167. https://doi.org/10.1083/jcb.109.5.2157

Shwartz, A., N. Dhanyasi, E.D. Schejter, and B.Z. Shilo. 2016. The Drosophila formin Fhos is a primary mediator of sarcomeric thin-filament array assembly. *eLife.* 5:e16540. https://doi.org/10.7554/eLife.16540

Verheyen, E.M., and L. Cooley. 1994. Profilin mutations disrupt multiple actin-dependent processes during Drosophila development. *Development.* 120:717–728.